



# Aerosol and physical atmosphere model parameters are both important sources of uncertainty in aerosol ERF

Leighton Regayre<sup>1</sup>, Jill Johnson<sup>1</sup>, Masaru Yoshioka<sup>1</sup>, Kirsty Pringle<sup>1</sup>, David Sexton<sup>2</sup>, Ben Booth<sup>2</sup>, Lindsay Lee<sup>1</sup>, Nicolas Bellouin<sup>3</sup>, and Kenneth Carslaw<sup>1</sup>

<sup>1</sup>Institute for Climate and Atmospheric Science, School of Earth and Environment, University of Leeds, Leeds, LS2 9JT, UK.

<sup>2</sup>UK Hadley Centre Met Office, Exeter, Fitzroy Road, Exeter, Devon, EX1 3PB, UK.

<sup>3</sup>Department of Meteorology, School of Mathematical & Physical Sciences, Faculty of Science, University of Reading, Reading, RG6 6BB, UK.

Correspondence to: Leighton Regayre (L.A.Regayre@leeds.ac.uk)

1 **Abstract.** Changes in aerosols cause a change in net top-of-the-atmosphere (ToA) short-wave and long-wave radiative fluxes,  
2 rapid adjustments in clouds, water vapour and temperature, and cause an effective radiative forcing (ERF) of the planetary  
3 energy budget. The diverse sources of model uncertainty and the computational cost of running climate models make it diffi-  
4 cult to isolate the main causes of aerosol ERF uncertainty and to understand how observations can be used to constrain it. We  
5 explore the aerosol ERF uncertainty by using fast model emulators to generate a very large set of aerosol-climate model vari-  
6 ants that span the model uncertainty due to twenty-seven parameters related to atmospheric and aerosol processes. Sensitivity  
7 analyses shows that the uncertainty in the ToA flux is dominated (around 80%) by uncertainties in the physical atmosphere  
8 model, particularly parameters that affect cloud reflectivity. However, uncertainty in the change in ToA flux caused by aerosol  
9 emissions over the industrial period (the aerosol ERF) is controlled by a combination of uncertainties in aerosol (around 60%)  
10 and physical atmosphere (around 40%) parameters. Four of the atmospheric and aerosol parameters that cause uncertainty in  
11 short-wave ToA flux (mostly parameters that directly scale cloud reflectivity, cloud water content or cloud droplet concentra-  
12 tions) also account for around 60% of the aerosol ERF uncertainty. The common causes of uncertainty mean that constraining  
13 the modelled planetary brightness to tightly match satellite observations changes the lower 95% credible aerosol ERF value  
14 from  $-2.65 \text{ W m}^{-2}$  to  $-2.37 \text{ W m}^{-2}$ . This suggests the strongest forcings (below around  $-2.4 \text{ W m}^{-2}$ ) are inconsistent with ob-  
15 servations. These results show that, regardless of the fact that the ToA flux is an order of magnitude larger than the aerosol ERF,  
16 the observed flux can constrain the uncertainty in ERF because their values are connected by constrainable process parameters.  
17 The key to reducing the aerosol ERF uncertainty further will be to identify observations that can additionally constrain indi-  
18 vidual parameter ranges and/or combined parameter effects, which can be achieved through sensitivity analysis of perturbed  
19 parameter ensembles.

## 20 1 Introduction

21 Large aerosol radiative forcing uncertainty has persisted through all Intergovernmental Panel on Climate Change assessment  
22 reports since 1996 despite substantial developments in climate model complexity (Flato et al. 2013, Section 9.1.3), numerous



23 intercomparison projects (Randles et al., 2013; Tsigaridis et al., 2014; Kim et al., 2014; Mann et al., 2014; Pan et al., 2015;  
24 Lacagnina et al., 2015; Kipling et al., 2016; Ghan et al., 2016; Koffi et al., 2016), and enormous investments in observing  
25 systems (Khain et al., 2000; Lacagnina et al., 2015; Seinfeld et al., 2016; Reddington et al., 2017). Reducing aerosol forcing  
26 uncertainty has therefore proven to be one of the most challenging and persistent problems in atmospheric science.

27

28 Reduction of uncertainty in aerosol effective radiative forcing (ERF) is an important objective, not least because it would  
29 improve climate change projections (Andreae et al., 2005; Myhre et al., 2013; Collins et al., 2013; Tett et al., 2013; Seinfeld  
30 et al., 2016). An improved understanding of the causes of uncertainty would also help to prioritise model developments, sug-  
31 gest fruitful analyses across multiple models, and point to potential new observations to constrain the uncertainties. However,  
32 the task remains challenging for multiple reasons. For example, aerosol ERF is usually quantified with reference to a period  
33 pre-dating the satellite era (usually 1850 or 1750) meaning it is not a directly observable quantity. Satellite-derived observations  
34 of present-day aerosol-cloud relationships have the potential to constrain the aerosol ERF uncertainty, but require an improved  
35 understanding of aerosol changes over the industrial period (Gryspeerd et al., 2017). Some of the ERF uncertainty might  
36 therefore be irreducible unless pristine present-day environments are shown to be a good proxy for pre-industrial conditions  
37 (Carslaw et al., 2013; Hamilton et al., 2014; Carslaw et al., 2017). Furthermore, aerosol ERF depends on many poorly under-  
38 stood interactions of aerosols with components of the physical climate system. Important sources of uncertainty are known  
39 to be aerosol emission fluxes (Granier et al., 2011), representations of complex sub-grid processes such as clouds (Haerter  
40 et al., 2009; Lohmann and Ferrachat, 2010; Guo et al., 2013; Gettleman et al., 2013; Golaz et al., 2013; Neubauer et al., 2014;  
41 Lohmann, 2017), precipitation responses (Tost et al., 2010; Croft et al., 2012; Michibata and Takemura, 2015), aerosol pro-  
42 cesses (Croft et al., 2012; Textor et al., 2006, 2007; Storelvmo et al., 2009; Kasoar et al., 2016), radiation calculations (Stier  
43 et al., 2013; Wilcox et al., 2015) and subsequent feedbacks on atmospheric dynamics (Booth et al., 2012; Bollasina et al., 2013;  
44 Kirtman et al., 2013; Villarini and Vecchi, 2013; Allen et al., 2014) and surface temperatures (Golaz et al., 2013).

45

46 Our intention here is to constrain aerosol ERF uncertainty by pursuing a ‘bottom-up’ approach that explores the underlying  
47 process uncertainty. This approach provides a set of observationally plausible model variants with which near-term climate  
48 simulations could be performed. Although a lower limit to the global mean aerosol ERF might be found using a ‘top-down’  
49 approach and historical temperature trends (Stevens, 2015), inferences made about the climate system are very sensitive to the  
50 simplifying assumptions that are made in top-down approaches (Knutti et al., 2008; Kretzschmar et al., 2017). More impor-  
51 tantly, such methods do not provide a model with which to make improved climate projections and they provide no information  
52 about regional variations in forcing, which are known to be important drivers of climate variability (Chalmers et al., 2012; Dun-  
53 stone et al., 2013; Shindell et al., 2013; Kirtman et al., 2013; Bollasina et al., 2013). Therefore, bottom-up methods that quantify  
54 aerosol ERF using global climate models whose performance and uncertainty are constrained by observations are required.

55

56 Multi-model studies (or model intercomparison projects, MIPs) can provide some information about ERF uncertainty be-  
57 cause a set of models with different dynamical cores and physical process parametrisations produces a range of aerosol re-



58 sponses. However, such opportunistic sampling has three main disadvantages. Firstly, inter-model comparisons often include  
59 models with vastly different degrees of complexity (Collins et al., 2013). For example, aerosol indirect effects are not repre-  
60 sented in many of the models included in such studies and this artificially inflates multi-model forcing uncertainty (Bellucci  
61 et al., 2017). Secondly, multiple members of an inter-model comparison will share key modules and behaviours (Pennell and  
62 Reichler, 2010; Collins et al., 2010; Knutti et al., 2013). This leads to compensating effects between groups of models with  
63 shared structural errors that causes the multi-model mean to outperform the majority of individual models across a range of  
64 climate metrics (Rougier, 2016). Thirdly, a small set of models (perhaps around twenty) cannot possibly sample the effects of  
65 dozens of interacting uncertain processes in the individual models (Carslaw et al., 2018). Therefore, inter-model comparisons  
66 do not provide statistically representative samples (Sexton et al., 2012; Knutti et al., 2013; Collins et al., 2013), making it  
67 difficult to draw inferences about the causes of aerosol ERF uncertainty and the robustness of any observational constraint.  
68 Leading experts subjectively assess the uncertainty in aerosol forcing as being larger than that quantified by multi-model stud-  
69 ies (Morgan et al., 2006).

70

71 A complementary approach to exploring aerosol ERF uncertainty in multiple models is to systematically explore the uncer-  
72 tain in underlying parameters and processes within a single model. Much progress has been made in understanding the causes  
73 of uncertainty in state variables related to aerosol ERF, such as cloud-active aerosol concentrations (Lee et al., 2011, 2012,  
74 2013; Samset et al., 2014; Mann et al., 2014; Shrivastava et al., 2016; Kipling et al., 2016), precipitation (Lebo and Feingold,  
75 2014; Qian et al., 2015; Johnson et al., 2015) and ToA radiative fluxes (Shiogama et al., 2012; Zhou et al., 2013; Randles et al.,  
76 2013). Furthermore, important sources of aerosol forcing uncertainty (in the absence of rapid atmospheric adjustments) have  
77 been identified (Schulz et al., 2006; Haerter et al., 2009; Lohmann and Ferrachat, 2010; Carslaw et al., 2013; Myhre et al.,  
78 2013; Regayre et al., 2014, 2015). However, no study has comprehensively explored aerosol ERF uncertainty in a model that  
79 accounts for rapid atmospheric adjustments. Studies that do include rapid adjustments (e.g. Gettleman, 2015) rely on one-at-a-  
80 time experiments (where individual parameters or model structures are perturbed in isolation) which do a poor job of sampling  
81 the model uncertainty because they neglect important parameter interactions (Pianosi et al., 2016).

82

83 Here we present a perturbed parameter ensemble of the HadGEM3-GA4-UKCA global aerosol-chemistry-climate model  
84 and use model emulation (Lee et al., 2013) to enable the combined effects of uncertainties in 27 aerosol, cloud and other atmo-  
85 spheric model processes to be quantified. Compared to our previous studies (Carslaw et al., 2013; Regayre et al., 2014, 2015)  
86 we take a more holistic approach to exploring model forcing uncertainty here by accounting for both the uncertainty in cloud  
87 and other physical atmospheric processes, as well as the uncertainties in the aerosol component of the model. We also explore  
88 for the first time the uncertainty in aerosol ERF (including rapid atmospheric adjustments to aerosols), and in the components  
89 of ERF from aerosol-radiation interactions ( $ERF_{ARI}$ ) and aerosol-cloud interactions ( $ERF_{ACI}$ ). Other attempts to quantify the  
90 uncertainty in the ToA radiative flux caused by aerosols (Tett et al., 2013; Shiogama et al., 2012) explored only the current  
91 state of the atmosphere and not how it changes over time.

92



93 The main questions we address in this paper are: 1) How much of the uncertainty in aerosol ERF is caused by aerosol  
94 processes and how much by physical atmosphere processes? The answer is important because it will tell us how the tuning of  
95 model processes apparently unrelated to aerosols might inadvertently affect the aerosol ERF that models calculate. 2) What  
96 are the processes that cause uncertainty in the aerosol ERF and to what extent do they also affect the observable radiative state  
97 of the atmosphere? This is important because aerosol ERF uncertainty will only be effectively constrained by observations if  
98 the uncertainty in both the ERF and the observations are driven by the same uncertain processes (Lee et al., 2016). 3) How  
99 much does tuning the radiative state of the model (i.e., ruling out implausible model settings) affect the range of aerosol ERFs?  
100 The effect of tuning of, for example, ToA radiative flux (Lohmann and Ferrachat, 2010; Mauritsen et al., 2012) on the aerosol  
101 ERF is not normally considered. However, we show that many model variants (and parts of uncertain parameter space) can  
102 be ruled out using ToA flux observations and that such state variable observations can play an important part in reducing the  
103 overall uncertainty in aerosol ERF. The results from this paper inform our more comprehensive effort to constrain aerosol ERF  
104 uncertainty using multiple observational quantities (Johnson et al., 2018).

105

106 In Section 2 we outline our methodology, then in Section 3.1 we quantify the magnitude of the uncertainty in aerosol ERF,  
107  $ERF_{ARI}$  and  $ERF_{ACI}$  through comprehensive sampling of model parameter uncertainty. We then analyse the main causes of  
108 uncertainty in aerosol ERF over multi-century and multi-decadal periods in Section 3.2 and the causes of ToA radiative flux  
109 uncertainty in Section 3.3 using sensitivity analysis techniques (Section 2). We also quantify the relative importance of atmo-  
110 spheric and aerosol parameters as sources of uncertainty in aerosol ERF and ToA radiative flux in Section 3.3. In Section 3.4 we  
111 identify the main causes of uncertainty in aerosol ERF and its components within 11 climatically important regions. Following  
112 Lohmann and Ferrachat (2010), we then explore how constraint of the model state using present-day ToA flux observations  
113 influences the plausible range of aerosol ERF (Sections 3.5.1 and 3.5.4). We show that while the relationships between the  
114 important driving parameters and individual parameter ranges are well constrained by ToA flux measurements (Sections 3.5.2  
115 and 3.5.3), the range of credible aerosol ERFs is only moderately (10%) constrained. We investigate the causes of the modest  
116 constraint in sections 3.5.2, 3.5.3 and 4.

117

## 118 2 Methods

### 119 2.1 Set-up of the HadGEM-UKCA aerosol-climate model

120 We used the UK Hadley Centre Met Office Unified Model (HadGEM3, 2017) including release version 8.4 of the UK Chemistry  
121 and Aerosol (UKCA) model, within which the evolution of particle size distribution and size-resolved chemical composition  
122 of aerosols are calculated using the GLObal Model of Aerosol Processes (GLOMAP; Spracklen et al., 2005; Mann et al.,  
123 2010). The model has a  $1.25^\circ \times 1.875^\circ$  horizontal resolution and 85 vertical hybrid pressure levels. The aerosol size distribution  
124 is defined by seven log-normal modes: one soluble nucleation mode as well as soluble and insoluble Aitken, accumulation  
125 and coarse modes. The aerosol chemical components are sulphate, sea salt, black carbon, particulate organic carbon and dust.



126 Secondary organic aerosol material is produced from the first stage oxidation products of biogenic monoterpenes under the as-  
127 sumption of zero vapour pressure. After kinetic condensation onto existing aerosols organic aerosols (primary and secondary)  
128 are treated as one chemical tracer.

129

130 The GLOMAP model resolves new particle formation, particle coagulation, gas-to-particle transfer, cloud processing (aque-  
131 ous chemistry) and the deposition of gases and aerosols. Sulphate particles form by binary homogeneous nucleation (Vehkamäki  
132 et al., 2002) throughout the atmosphere and by organically-mediated nucleation (Metzger et al., 2010) in the boundary layer.  
133 The activation of aerosol particles into cloud droplets is calculated using distributions of sub-grid vertical velocities (West  
134 et al., 2014) and the removal of cloud droplets by autoconversion into rain drops is calculated by the physical atmosphere  
135 model. Aerosol removal by impaction scavenging of falling raindrops (within and below clouds) in the physical atmosphere  
136 model depends partly on the collocation of clouds and precipitation (Boutle et al., 2014). Soluble particles grow according to  
137 the relative atmospheric humidity using composition dependent hygroscopicity factors ( $\kappa$ ) in accordance with ‘Köhler theory’  
138 (Petters and Kreidenweis, 2007).

139

140 Successive versions of the GLOMAP model have been widely evaluated against global measurements of particle number  
141 concentration (Spracklen et al., 2010; Reddington et al., 2011), chemical compositions (Spracklen et al., 2011b; Schmidt et al.,  
142 2011; Browse et al., 2012) and cloud active aerosol concentrations (Korhonen et al., 2008; Spracklen et al., 2011a; Pringle  
143 et al., 2012). The HadGEM models are subject to constant monitoring for ongoing use in numerical weather prediction and  
144 have informed successive Coupled Model Inter-comparison Project (CMIP) experiments (Taylor et al., 2012). HadGEM ca-  
145 pably represents changes in cloud regime (Nam et al., 2012); one of the requirements for simulating rapid adjustments to  
146 aerosol perturbations (Stevens and Feingold, 2009; Zhang et al., 2015). Cloud water responses to aerosols may be too strong  
147 in the HadGEM model because the current model version does not represent enhanced drying in polluted clouds (Torrence and  
148 Compo, 1998). However, over multiple cloud regimes the cloud water response is not of a sufficient magnitude to be climati-  
149 cally important (Malavelle et al., 2017).

150

151 Anthropogenic emission scenarios prepared for the Atmospheric Chemistry and Climate Model Inter-comparison Project  
152 (ACCMIP; Lamarque et al., 2010) and prescribed in some of the CMIP Phase 5 experiments (Taylor et al., 2012) are pre-  
153 scribed here. Carbonaceous aerosol emissions from fires were prescribed using a ten year average of 2002 to 2011 monthly  
154 mean data from the Global Fire and Emissions Database (GFED3; van der Werf et al., 2010).

155

156 Model horizontal winds were relaxed (nudged) towards winds from the European Centre for Medium-Range Weather Fore-  
157 casts (ECMWF) ERA-Interim reanalysis above around 2 km. Nudging of atmospheric states is used primarily to evaluate  
158 output from global models (Telford et al., 2008) or to ensure that pairs of simulations have near-identical atmospheric states,  
159 so that aerosol and/or chemistry perturbations can be applied and their effects quantified using single realisations of each simu-  
160 lation. In ‘free-running’ (non-nudged) simulations radiative fluxes need to be averaged over many decades in order to produce



161 signals stronger than the noise resulting from internal variability (Kooperman et al., 2012). Nudging to horizontal winds above  
162 around 2 km forces synoptic-scale dynamical features to be consistent across the ensemble, whilst allowing boundary layer  
163 atmospheric adjustments in response to changes in aerosols to be affected by the parameter perturbations.

164

165 Each simulation was subject to a seven-month spin-up period from a consistent starting simulation, with parameters set to  
166 their median values for the first four months. Parameter perturbations were applied during the final three months of the spin-up  
167 period, after which a full year of data was produced for each ensemble member. Aerosol ERF is calculated as the difference in  
168 net ToA short-wave plus long-wave radiative fluxes between pairs of simulations with identical parameter settings but distinct  
169 prescriptions of anthropogenic emissions (1850, 1978 and 2008). The aerosol ERF and its components were calculated based  
170 on the method of Ghan (2013).

171

## 172 2.2 Parameter sampling

173 The 27 parameters perturbed in the ensemble, as well as the roles they play in the model, are presented in Table A1. We per-  
174 turbed 9 parameters in the physical atmosphere model known to affect the properties and distribution of clouds and humidity  
175 within the boundary layer (*atmospheric parameters*; Sexton et al. 2018) in combination with 18 aerosol emission, deposition  
176 and process parameters (*aerosol parameters*) known to affect cloud droplet number concentrations (Lee et al., 2013) and/or  
177 aerosol cloud-albedo effect forcing (the  $ERF_{ACI}$  without accounting for rapid adjustments) at the global (Carslaw et al., 2013;  
178 Regayre et al., 2014) and/or regional scale (Regayre et al., 2015). Some parameters have been included in the ensemble because  
179 they represent model structural advances with inherent process uncertainty (Yoshioka et al., In prep.).

180

181 We did not attempt to include an exhaustive set of uncertain parameters in the experimental design. Current supercomputing  
182 resources are too valuable to justify an uninformed, exhaustive exploration of model uncertainty. Instead, we used one-at-a-time  
183 perturbation screening experiments (not shown) to identify the parameters most likely to influence radiative forcing within the  
184 model. The parameters included in the preliminary screening process were identified by model experts as the key parameters  
185 within individual model schemes (e.g. cloud microphysics) and/or model processes (e.g. cloud droplet activation) with the  
186 potential to significantly affect aerosol ERF.

187

188 The parameters we perturb here are likely to have readily identifiable counterparts in other climate models. All global cli-  
189 mate models have similarities because they describe the same physical processes and although process parametrisations can  
190 differ between models they often share common biases when compared to measurements (Knutti et al., 2013). Therefore, our  
191 aim to identify the main causes of aerosol ERF uncertainty in the HadGEM model (Section 3) will provide valuable clues for  
192 reducing the aerosol ERF uncertainty in other models.

193





## 194 2.2.1 Definition of atmospheric parameters

195 **Rad\_Mcica\_Sigma:** *The fractional standard deviation of the sub-grid cloud condensate as seen by radiation.* This parameter  
196 controls the inhomogeneity of cloud condensate within vertically overlapping sub-grid clouds (Räisänen et al., 2004) which  
197 is used to calculate cloud radiative fluxes. Higher values of Rad\_Mcica\_Sigma increase cloud condensate inhomogeneity and  
198 hence reduce cloud albedo (because of the non-linear relationship between albedo and cloud condensate; Barker and Räisänen,  
199 2005). Atmospheric temperature profiles respond to changes in the cloud radiative fluxes and can induce changes in precipita-  
200 tion rates and cloud amount. The effect of perturbing Rad\_Mcica\_Sigma on reflected radiation is largest in regions of persistent  
201 stratocumulus cloud where low-altitude, high-albedo clouds occupy a substantial fraction of each model grid box.

202

203 **C\_R\_Correl:** *Cloud and rain sub-grid horizontal correlation.* The collocation of clouds and rain within the model is impor-  
204 tant because it determines the accretion rate of cloud droplets and aerosols by rain drops. Higher values cause more accretion  
205 because regions of high cloud water are closely correlated with regions of high precipitation. Perturbations to this parameter  
206 affect cloud radiative properties by altering in-cloud interstitial aerosol concentrations and cloud amount.

207

208 **Niter\_Bs:** *Number of microphysics iteration substeps.* The microphysical processing of in-cloud interstitial aerosols and  
209 cloud droplets is controlled by the cloud microphysics scheme within the physical atmosphere model. The values of this pa-  
210 rameter determine the degree of processing within a model timestep. Each iteration of the microphysics scheme allows drops  
211 to grow larger before precipitation occurs. Therefore, higher parameter values allow for greater microphysical processing and  
212 cause the model to produce less light rain. This affects the amount of liquid water within clouds and alters the amount of cloud  
213 which is important for cloud radiative effects.

214

215 **Ent\_Fac\_Dp:** *Entrainment amplitude scale factor.* This convection scheme parameter controls the shape of the convective  
216 mass flux and the sensitivity of convection to relative humidity. Higher values reduce the depth of convection and suppress  
217 convective precipitation. This parameter is important for cloud radiative effects for several reasons. First, the retention of cloud  
218 water increases cloud amount and short-wave reflectivity. Second, lower altitude clouds have a higher cloud top temperature  
219 and attenuate less of the long-wave energy emitted by the Earth's surface. Third, if atmospheric moisture is not precipitated  
220 convectively, the increase in relative humidity causes more large-scale, frontal precipitation which affects spatial distributions  
221 of aerosols and clouds and hence the aerosol ERF.

222

223 **Amdet\_Fac:** *Mixing detrainment rate scale factor.* This parameter controls the rate of humidification of the atmosphere  
224 and the shape of the convective heating profile. Amdet\_Fac is important for cloud radiative effects for similar reasons to  
225 Ent\_Fac\_Dp. Both parameters affect clouds through their influence on convection but through different mechanisms. Higher  
226 values of Amdet\_Fac increase atmospheric humidity and temperature leading to enhanced convection.

227



228 **Dbsdtbs\_Turb\_0:** *The cloud erosion rate.* This parameter alters the radiative properties of clouds by altering the rate at  
229 which unresolved sub-grid motions mix clear and cloudy air. Higher values cause more rapid mixing of clear, dry air into  
230 clouds, thereby reducing cloud liquid water content, autoconversion of cloud droplets to rain drops and cloud amount. The  
231 atmospheric lifetimes of aerosols and precursor gases are noticeably affected by this parameter.

232

233 **Mparwtr:** *Maximum value of the function controlling convective parcel maximum condensate.* Convective parcels near the  
234 Earth's surface precipitate when the amount of moisture reaches the threshold set by this parameter. Higher values increase  
235 cloud amount and lifetime by reducing convective precipitation. As with other convective parameters Mparwtr affects cloud  
236 radiative effects and aerosols by altering the spatial distributions of clouds and precipitation.

237

238 **Dec\_Thres\_Cld:** *The threshold for cloudy boundary layer decoupling.* Boundary layer stability plays an important role in  
239 determining the magnitude of cloud radiative effects because a well-mixed, stable boundary layer retains more heat and permits  
240 more dynamic activity. This parameter is the threshold at which the boundary layer decouples from the rest of the atmosphere.  
241 Hence, higher parameter values lead to a more well-mixed boundary layer, increased cloudiness and longer in-cloud processing  
242 times for aerosols.

243

244 **Fac\_Qsat:** *Rate of change of convective parcel maximum condensate with altitude.* The maximum amount of moisture a con-  
245 vective parcel can hold transitions from the threshold set by the parameter Mparwtr at the surface to a much smaller threshold  
246 at high altitudes. Fac\_Qsat controls the rate at which this threshold changes with altitude. Fac\_Qsat therefore influences cloud  
247 radiative effects through similar mechanisms to Mparwtr (higher values suppress precipitation and increase cloud amount and  
248 lifetime) but is more important in the upper boundary layer.

249

### 250 2.2.2 Definition of the aerosol parameters

251 **Ageing:** *Ageing of hydrophobic aerosols.* Carbonaceous aerosols are assumed to be non-hygroscopic when emitted into the  
252 atmosphere and cannot act as cloud condensation nuclei until sufficient layers of sulphuric acid and condensible organic mat-  
253 ter coat their surface. This parameter is the number of monolayers of soluble material required to convert initially insoluble  
254 aerosols into cloud condensation nuclei. Higher values reduce the conversion rate of hydrophobic to hygroscopic aerosols. This  
255 parameter is important for aerosol ERF because it affects cloud condensation nuclei and the removal rate of highly-absorbing  
256 carbonaceous aerosols from the atmosphere.

257

258 **Cloud\_pH:** *pH of cloud droplets.* The pH of cloud droplets is used in the aqueous chemistry module of GLOMAP to cal-  
259 culate the conversion of SO<sub>2</sub> into sulphate particles. Cloud droplet pH depends on kinetic and thermodynamic processes that  
260 are not explicitly simulated. Therefore, we use a globally defined value of cloud droplet pH to control the reaction rate. Un-  
261 certainty in this parameter accounts for the simplification in its application. Higher values of this parameter increase sulphate





262 production near  $\text{SO}_2$  emission sites and tend to reduce aerosol concentrations in remote regions (through effects on new parti-  
263 cle formation). Therefore, the cloud pH parameter affects the spatial distribution of aerosols which is important for aerosol ERF.  
264

265 **Carb\_BB\_Ems:** *Carbonaceous biomass burning emission scale factor.* Higher values of this scale factor increase the  
266 amount of carbonaceous aerosols emitted into the atmosphere from large-scale biomass burning. Carbonaceous aerosols are  
267 important for aerosol ERF because they absorb solar radiation and the resulting energy redistribution affects boundary layer  
268 temperatures and stability and can affect cloud cover (Gnanadesikan et al., 2017).  
269

270 **Carb\_BB\_Diam:** *Carbonaceous biomass burning emission diameter (nm).* This parameter determines the size of carbona-  
271 ceous aerosols at time of emission. Higher values cause fewer, larger carbonaceous aerosols to be emitted for a given value  
272 of Carb\_BB\_Ems. Therefore, the total carbonaceous aerosol particle number is reduced, leading to fewer cloud condensation  
273 nuclei and a change in aerosol optical properties.  
274

275 **Sea\_Spray:** *Sea spray aerosol emission scale factor.* Aerosol ERF is sensitive to emission fluxes of natural aerosols because  
276 they strongly influence the pre-industrial background aerosol concentration and the relative magnitude of the change in aerosols  
277 over the industrial period. Perturbations to the wind-driven emission fluxes affect aerosol distributions in marine and coastal  
278 regions.  
279

280 **Anth\_SO2:** *Anthropogenic  $\text{SO}_2$  emission scale factor.*  $\text{SO}_2$  gas forms  $\text{H}_2\text{SO}_4$  molecules which condense to form sulphate  
281 particles. Furthermore,  $\text{SO}_2$  condenses onto existing particles increasing their size and solubility. Therefore, scaling anthro-  
282 pogenic  $\text{SO}_2$  emissions affects aerosol ERF by influencing the concentrations and composition of present-day aerosols.  
283

284 **Volc\_SO2:** *Volcanic  $\text{SO}_2$  emission scale factor.* Volcanic  $\text{SO}_2$  emissions are treated identically to anthropogenic  $\text{SO}_2$  emis-  
285 sions. However, they are present in both the pre-industrial and present-day atmospheres so exert an influence on aerosol ERF  
286 through a similar mechanism as Sea\_Spray by altering the pre-industrial aerosol concentration.  
287

288 **BVOC\_SOA:** *Biogenic secondary aerosol formation from volatile organic compounds scale factor.* Secondary organic  
289 aerosols form through multi-stage oxidation reactions of biogenic volatile organic compounds (monoterpenes in this case).  
290 This parameter scales the secondary organic aerosol emission flux, with higher values producing larger emissions. Perturbing  
291 this parameter changes the aerosol concentration and size distribution in the pre-industrial and present-day atmosphere.  
292

293 **DMS:** *Dimethylsulphide surface ocean concentration scale factor.* Perturbing the concentration of DMS in the oceans alters  
294 the wind-driven flux of DMS into the atmosphere. DMS is important for aerosol ERF because it is a source of natural aerosols  
295 which affect the pre-industrial aerosol background concentrations. Similar to the Sea\_Spray parameter, DMS affects aerosol  
296 concentrations in marine and coastal regions. However, marine DMS concentrations increase with ocean temperature so per-



297 turbations to this parameter will have the greatest influence on aerosol ERF in warmer months.

298

299 **Dry\_Dep\_Acc:** *Accumulation mode dry deposition velocity scale factor.* Aerosols are removed from the atmosphere at a  
300 velocity calculated using Brownian diffusion, impaction and interception. This calculation in the GLOMAP model depends on  
301 wind speeds and surface roughness. High values of this parameter more readily remove accumulation mode aerosols from the  
302 atmosphere causing a reduction in cloud condensation nuclei concentrations.

303

304 **Dry\_Dep\_SO2:** *SO<sub>2</sub> dry deposition velocity scale factor.* This parameter determines the removal of SO<sub>2</sub> gas from air masses  
305 that interact with the surface. The removal of SO<sub>2</sub> is important for aerosol ERF because SO<sub>2</sub> is a precursor for sulphate parti-  
306 cles and condenses onto existing particles causing them to grow to the larger sizes needed to act as cloud condensation nuclei.  
307 Higher values of this parameter increase the removal rate of SO<sub>2</sub> from the atmosphere. This affects aerosol size distributions  
308 by simultaneously reducing particle formation rates and the growth rates of existing aerosols.

309

310 **Kappa\_OC:** *Köhler coefficient of organic carbon.* Aerosol water uptake efficiency is determined by ‘Köhler theory’ using  
311 size and composition dependent hygroscopicity factors ( $\kappa$ ; Petters and Kreidenweis, 2007). Higher values of this parameter  
312 increase the water uptake efficiency of the organic material in the particles. Perturbations to this parameter will change the  
313 light-scattering efficiency of the particles and the droplet activation process, thereby affecting cloud microphysical processes.  
314 In particular, cloud-active aerosol concentrations in the pre-industrial atmosphere are expected to be susceptible to this param-  
315 eter value (Liu and Wang, 2010).

316

317 **Sig\_W:** *Updraft vertical velocity standard deviation.* This parameter controls the width of the probability distribution of  
318 sub-grid vertical velocities used to calculate the activation of aerosols into cloud droplets. Higher Sig\_W values widen the dis-  
319 tribution of updraft velocities. The largest sub-grid updrafts within the distribution have the greatest influence on cloud droplet  
320 concentrations because, for any given supersaturation, a larger updraft velocity will cause a greater proportion of relatively  
321 small aerosols to activate. Higher values of Sig\_W therefore increase cloud droplet concentrations, decrease precipitation ef-  
322 ficiency (through reduced autoconversion rates), cloud liquid water content and cloud albedo. Sig\_W perturbations have the  
323 greatest influence on cloud droplet concentrations in regions of relatively high aerosol concentrations because in such environ-  
324 ments droplet activation is updraft-limited rather than aerosol-limited.

325

326 **Dust:** *Dust emission scale factor.* Dust aerosols are large, insoluble particles when emitted, but are treated as hygroscopic  
327 once sufficiently aged by the condensation of soluble material onto the particle surface (as defined by the ‘ageing’ parameter).  
328 We perturb dust emissions in our ensemble because they are important for the ERF<sub>ARI</sub> component of aerosol ERF. Further-  
329 more, dust influences cloud-active aerosol concentrations (Manktelow et al., 2010) and cloud droplet concentrations (Karydis  
330 et al., 2017).

331



332 **Rain\_Frac:** *Fraction of cloud-covered area in large-scale clouds where scavenging occurs.* Rain and clouds do not correlate  
333 perfectly (as discussed in the C\_R\_Correl definition). Higher values of this parameter allow aerosols to be scavenged by rain  
334 drops over a greater fraction of cloudy areas. The value of this parameter is important for aerosol ERF because it affects aerosol  
335 atmospheric lifetimes.

336

337 **Cloud\_Ice\_Thresh:** *Threshold of cloud ice fraction above which nucleation scavenging of aerosol material is suppressed.*  
338 The scavenging of aerosol material in dynamic rain systems is controlled partly by the rain formation process - either collision-  
339 coalescence process that efficiently removes many aerosol particles in raindrops or the Wegener-Bergeron-Findeisen process  
340 in mixed-phase clouds, which leads to less aerosol scavenging and seems to account for the efficient winter-time transport of  
341 aerosols to the Arctic (Barrett et al., 2011; Browse et al., 2012). In our previous studies (Regayre et al., 2014, 2015) we de-  
342 fined a temperature below which scavenging was suppressed. Here, we instead use the mass fraction of ice to define a threshold  
343 above which no nucleation scavenging occurs. Higher values require a greater proportion of ice to be present before scavenging  
344 is suppressed. This parameter is important for high latitude aerosol concentrations and cloud radiative effects (Browse et al.,  
345 2012; Regayre et al., 2015; Yoshioka et al., In prep.).

346

347 **BC\_RI:** *Imaginary part of the black carbon refractive index.* This parameter controls the absorption of radiation as it passes  
348 through aerosols containing black carbon. Higher values of the imaginary refractive index cause more energy to be absorbed  
349 and re-emitted by black carbon aerosols. The real part of the refractive index is defined according to the imaginary part mean-  
350 ing that this parameter also controls the scattering of radiation by black carbon aerosols. Higher values of the real part cause  
351 more incoming radiation to be refracted towards the Earth's surface (more forward scattering). Perturbations to BC\_RI affect  
352  $ERF_{ARI}$  as well as the vertical profile of atmospheric heating and hence convection, cloud amount and cloud radiative effects.  
353 Our simulations do not account for effect of depositing light-absorbing carbonaceous aerosols on snow (Bond et al., 2013), nor  
354 the air-sea interactions that enhance rapid adjustments in marine regions (Gnanadesikan et al., 2017).

355

356 **OC\_RI:** *Imaginary part of the organic carbon refractive index.* The absorption of radiation by organic carbon is controlled  
357 by this parameter. Unlike BC\_RI, the real part of the organic carbon refractive index is held constant. Therefore, perturba-  
358 tions to this parameter have no effect on the refractive properties of organic carbon. Otherwise, OC\_RI affects the atmosphere  
359 through the same mechanisms as BC\_RI.

360

361 One potentially important parameter that we did not perturb is the autoconversion rate of cloud droplets into rain drops (al-  
362 though we did perturb Rain\_Frac and C\_R\_Correl which affect aerosol and cloud droplet removal by rain drops). The coupling  
363 between the GLOMAP model and the cloud microphysics scheme is currently one-way: cloud droplet concentrations calcu-  
364 lated in GLOMAP are used in the autoconversion scheme and thereby affect precipitation rates, cloud liquid water content and  
365 albedo. However, precipitation only alters the cloud droplet concentrations in HadGEM and not aerosol concentrations within  
366 the GLOMAP model. For aerosol concentrations to be directly altered by the autoconversion process, the coupling would need



367 to be two-way so that cloud droplet concentrations in GLOMAP were consistent with those calculated in the atmospheric  
368 model's microphysics scheme.

369

370 Other HadGEM simulations showed that over multiple cloud regimes cloud liquid water path is not substantially affected  
371 by aerosols through autoconversion (Malavelle et al., 2017), suggesting that neglecting the uncertainty in this process is not  
372 important to our results. However, in relatively polluted regions (such as the North Atlantic) cloud liquid water path responses  
373 to aerosols in low-altitude clouds (particularly Stratocumulus) are likely to be overestimated in the model because of known  
374 structural errors (Torrence and Compo, 1998). Despite this, the cloud liquid water path response to aerosols in low, warm  
375 clouds is weaker in HadGEM than in other global climate models (Ghan et al., 2016). Therefore, autoconversion may be more  
376 important in other models, but will likely be overstated (Torrence and Compo, 1998). This process should be considered in fu-  
377 ture uncertainty analysis studies once shared model structural errors are addressed and the process uncertainty better quantified.  
378

### 379 2.3 Statistical methodology

380 Maximin Latin Hypercube sampling was used to create a parameter combination design of 162 points with excellent space-  
381 filling properties that provide information on model output across the 27-dimensional parameter uncertainty space. A sim-  
382 ulation with all parameters set to their median values (from distributions described in table A1) was also included in the  
383 ensemble. Emulators were then constructed which describe individual model outputs (e.g., ToA flux, aerosol ERF) over the  
384 27-dimensional space of the uncertain parameters. Emulators provide a statistical representation of model output for all points  
385 within the multi-dimensional parameter space and have been widely used to analyse climate models (Lee et al., 2013; Carslaw  
386 et al., 2013; Tett et al., 2013; Regayre et al., 2014; Hamilton et al., 2014; Regayre et al., 2015; Johnson et al., 2015; Lee et al.,  
387 2016) as well as complex models in many other areas of science, including hydrology (Liu and Gupta, 2007), galaxy formation  
388 (Rodrigues et al., 2017) and disease transmission (Andrianakis et al., 2017).

389

390 In total 217 perturbed parameter simulations were created for each anthropogenic emission period including a set of 54  
391 simulations with parameter combinations that augment the original design and were used to validate the emulators. Twenty-six  
392 simulations did not complete an annual cycle in at least one of the anthropogenic emission periods (1850, 1978 and 2008)  
393 because the combinations of parameters caused the model to fail. Hence, the ensemble of simulations for each period was  
394 made up of the remaining 191 simulations. Once emulators were validated, new emulators conditioned on output from the 191  
395 perturbed parameter simulations (with better space-filling properties) were created by combining the validation simulations  
396 with the original set of simulations.

397

398 Probability density functions (pdfs; Table A1) were used to represent expert beliefs about parameter uncertainty. We pre-  
399 dominantly used trapezoidal distributions (Hetzl, 2012) to represent parameter uncertainty in order to avoid having an overly-



400 centralized multi-variate sample (Yoshioka et al., In prep.).

401

402 By combining perturbed parameter ensembles with model emulation and then densely sampling emulator output using the  
403 extended-FAST sampling method (Saltelli et al., 1999), we were able to perform sensitivity analyses (Saltelli et al., 1999, 2000;  
404 Lee et al., 2012) and decompose the variance in model output into individual components. We used the percentage reduction  
405 in variance which would be achieved if a parameter value was known exactly as our main statistic for identifying the causes of  
406 uncertainty. Emulation and sensitivity analyses were applied at the individual model gridbox level (degraded to N96 model res-  
407 olution) as well as at the regional and global mean level. For the sensitivity analyses, samples of 270000 members were drawn  
408 from the emulators at parameter combinations determined by the parameter pdfs. The sensitivity analysis results are therefore  
409 informed by expert knowledge about the model behaviour in relation to the uncertain processes. However, for the constraint of  
410 aerosol ERF using ToA flux observations we sampled one million model variants using uniform pdfs. This sampling approach  
411 uses the expert-elicited parameter pdfs to determine the ranges of uniform pdfs for sampling but neglects expert prior beliefs  
412 about parameter value likelihoods. As such, the effects of applying the observational constraint and expert knowledge can be  
413 quantified and compared. Furthermore, the effect of applying the observational constraint on the uncertain parameter space can  
414 be more readily assessed when uniform pdfs are used to create the original sample because parameter combinations are more  
415 evenly spaced throughout the 27-dimensional parameter space.

416

417 Preliminary parameter combination screening tests revealed that values of Ent\_Fac\_Dp higher than around 1.8 in combi-  
418 nation with values of Amdet\_Fac higher than around 8.0 caused model simulations to fail. This part of the 27-dimensional  
419 parameter space (a corner of a 2D plane) was removed from the ensemble design and analyses. The sampling method used to  
420 perform the sensitivity analyses, was adapted to reject samples from the 2D corner of parameter space not included in the de-  
421 sign. Rejected combinations of the Ent\_Fac\_Dp and Amdet\_Fac parameters were re-sampled from the restricted 2D parameter  
422 space without affecting the sampling frequency across the remaining 25-dimensional parameter space.

423

## 424 3 Results

### 425 3.1 Uncertainty in aerosol ERF and its components

426 Figure 1 shows pdfs of the global mean aerosol ERF (from 1850 to 2008) and its components;  $ERF_{ARI}$  and  $ERF_{ACI}$ . The 95%  
427 credible interval of aerosol ERF used in the sensitivity analysis is  $-2.18$  to  $-0.71 \text{ W m}^{-2}$ . Most of the uncertainty in aerosol  
428 ERF comes from the  $ERF_{ACI}$  component, which has a credible interval of  $-2.20$  to  $-0.61 \text{ W m}^{-2}$  and captures much of the  
429 recognised uncertainty in this forcing term (Myhre et al., 2013; Shindell et al., 2013). We also account for above-cloud aerosols  
430 (Ghan, 2013) in our calculation of  $ERF_{ACI}$  and  $ERF_{ARI}$  which affects the balance between these two components of aerosol  
431 ERF (Yoshioka et al., In prep.). This adjustment results in distributions of weaker  $ERF_{ARI}$  values and stronger  $ERF_{ACI}$  values



432 in our sample compared to (Myhre et al., 2013). We discuss these effects further in Section 3.1.2.

433

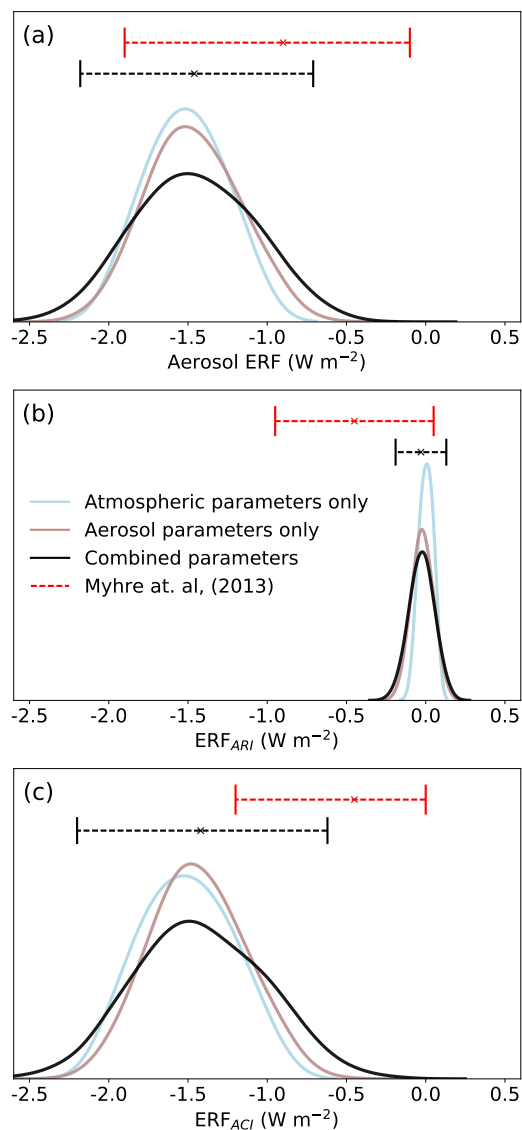


**Figure 1.** Probability density functions of 1850-2008 (a) aerosol ERF, (b)  $\text{ERF}_{ARI}$  and (c)  $\text{ERF}_{ACI}$ . Each sample contains 270000 emulator-derived model variants informed by the expert-elicited prior probability distributions of parameter values. Samples with aerosol and atmospheric parameter uncertainties neglected (Table A1) were obtained by setting each neglected parameter to its median value in the corresponding pdf. 90% credible intervals from (Myhre et al., 2013) are presented as red horizontal lines with best estimates marked using crosses. Our 95% credible intervals are presented in black and the sample median is presented using a cross.





434 The sample of aerosol ERFs in Fig. 1 has already been constrained by our choice of probability distributions for the uncer-  
435 tain parameters (Table A1). When we use uniform parameter distributions to sample parameter combinations (Section 2.3) the  
436 credible range (95%) of aerosol ERFs is  $-2.65$  to  $-0.68$   $\text{W m}^{-2}$ . By applying expert beliefs about parameter value likelihoods  
437 the aerosol ERF credible range is only  $-2.18$  to  $-0.71$   $\text{W m}^{-2}$  (Fig. 1(a)). This implies that by applying the combined knowledge  
438 of experts with an understanding of the model processes and parametrisations we have effectively reduced the aerosol ERF  
439 credible range by around 25%.

440

441 The strongest aerosol ERFs in our distribution would lead to a negative forcing when combined with best estimates of  
442 changes in other forcing agents over the industrial period. A net negative forcing is incompatible with the observed increase in  
443 global mean surface temperatures over the industrial period (e.g. HadCRUT4, 2017). However, there is substantial uncertainty  
444 in the ERFs of multiple other forcing agents (Myhre et al., 2013; Fig. 8.16 and 8.18) so our most negative aerosol ERF values  
445 cannot be considered implausible using this criteria. Structural aspects of the model could account for the strongest forcings.  
446 For example, our model is missing marine sources of organic aerosols and related processes (Gantt et al., 2015) which, if in-  
447 cluded, would act as an important source of ice-nucleating particles (Vergara-Temprado et al., 2017) and pre-industrial aerosols  
448 (Gordon et al., 2017) which would weaken the aerosol forcing (Carslaw et al., 2013). However, our perturbed parameter ranges  
449 were to some extent intended to encompass the uncertainty caused by those structural deficiencies we were aware of. The  
450 values in the tails of the aerosol ERF pdf are likely to be the result of setting multiple parameters important for aerosol ERF  
451 to extreme values, which are also likely to cause extreme present-day ToA flux values and be considered implausible when  
452 compared to observations (Sections 3.5).

453

454 Figure 1 also shows the separate effects of the 18 combined aerosol parameters and the 9 combined physical atmosphere  
455 model uncertainties. Neglecting the uncertainty in aerosol parameters (by setting them to their median values in the all model  
456 variants) results in a 95% credible aerosol ERF interval of  $-1.98$  to  $-1.04$   $\text{W m}^{-2}$ , while neglecting uncertainty in atmospheric  
457 parameters results in a credible interval of  $-2.00$  to  $-0.90$   $\text{W m}^{-2}$ . Summary statistics of forcing from these samples are pre-  
458 sented in Table A2. The distribution of aerosol ERF (as well as  $\text{ERF}_{ARI}$  and  $\text{ERF}_{ACT}$ ) is wider and flatter (has a larger  
459 variance) in the combined sample than the distributions of atmosphere-only and aerosol-only sampled values. This suggests  
460 that important interactions between atmospheric and aerosol parameters cause the most extreme aerosol ERF values. The ef-  
461 fects of the aerosol and physical model uncertainties do not have an additive effect on the aerosol ERF uncertainty because  
462 of compensating effects between the groups of parameters. These results show that both atmospheric and aerosol parameter  
463 perturbations are required to comprehensively sample model uncertainty. The main atmospheric and aerosol sources of aerosol  
464 ERF uncertainty are identified in Section 3.2.1.

465



### 466 3.1.1 Uncertainty in $ERF_{ACI}$

467 Maps of the means and standard deviations of  $ERF_{ACI}$  resulting from perturbations to our 27 atmospheric and aerosol pa-  
468 rameters are presented in Fig. 2. Forcings stronger than  $-3.5 \text{ W m}^{-2}$  are concentrated over anthropogenic aerosol sources  
469 (particularly Asia, America and Europe) and in marine stratocumulus regions (Atlantic Ocean, North Pacific Ocean and the  
470 South Pacific Ocean off the South American coast). The standard deviation of  $ERF_{ACI}$  is largest (up to  $6 \text{ W m}^{-2}$ ) in the same  
471 regions and is typically of the same order of magnitude as the mean regional value. The spatial distribution of mean  $ERF_{ACI}$  is  
472 very similar to the Atmospheric Chemistry and Climate Model Intercomparison Project (ACCMIP) multi-model mean pattern  
473 (Shindell et al., 2013). However, the magnitudes of forcing differ, particularly over remote marine regions. For example, our  
474 mean  $ERF_{ACI}$  is stronger than  $-5 \text{ W m}^{-2}$  over much of the North Pacific Ocean, whereas the ACCMIP mean aerosol ERF in the  
475 Pacific is stronger than  $-3.5 \text{ W m}^{-2}$  only in coastal regions near to anthropogenic sources. These strong remote marine  $ERF_{ACI}$   
476 values go some way to explaining the differences in global mean  $ERF_{ACI}$  between our sample (around  $-1.4 \text{ W m}^{-2}$ ) and the  
477 ACCMIP multi-model mean (around  $-0.9 \text{ W m}^{-2}$ ). In part, the magnitude of our  $ERF_{ACI}$  values are caused by the above-cloud  
478 aerosol adjustment (Ghan, 2013). Our model has a relatively weak cloud liquid water path response to aerosols (Ghan et al.,  
479 2016; Malavelle et al., 2017), which suggests that our very negative marine forcing values are not caused by an overly strong  
480 aerosol second indirect effect.

481

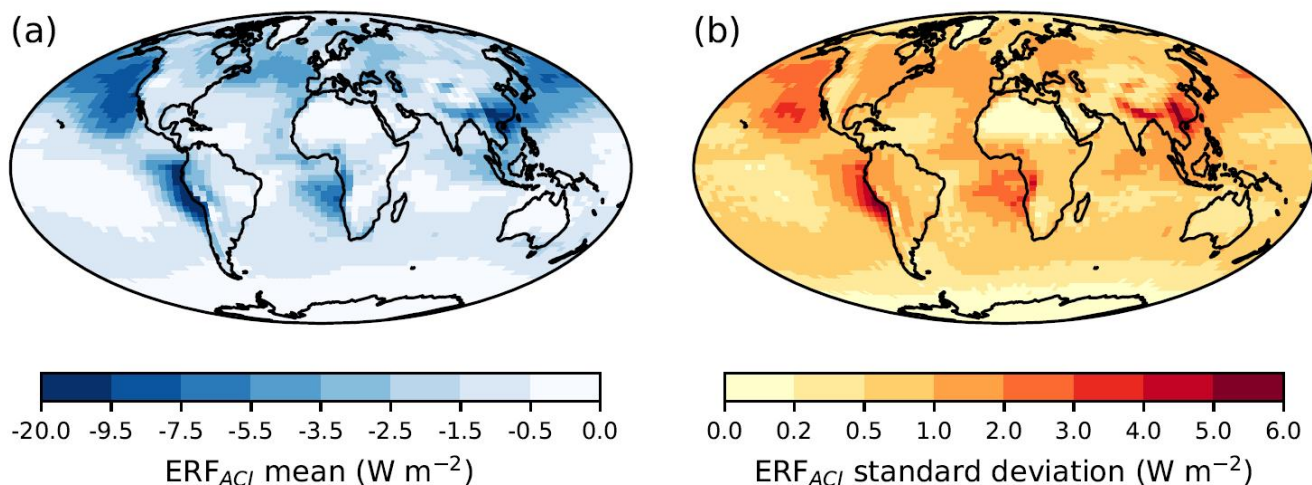


**Figure 2.** (a) Mean and (b) standard deviation for 1850-2008  $ERF_{ACI}$  forcing. Values were calculated using output from 270000 emulator-derived model variants at the individual pixel level once degraded to N96 model resolution. These samples of model variants are informed by the expert-elicited parameter pdfs.



### 482 3.1.2 Uncertainty in $ERF_{ARI}$

483 Fig. 3 shows the spatial pattern of mean  $ERF_{ARI}$  and its standard deviation. Global mean  $ERF_{ARI}$  is near zero (95% credible  
484 range  $-0.19$  to  $0.13 \text{ W m}^{-2}$ ; Fig. 1; Table A2). Although the possibility of a globally positive  $ERF_{ARI}$  has previously been con-  
485 sidered unlikely (Boucher et al., 2013), it has important implications for our understanding of interactions between absorbing  
486 aerosols, cloud-processes and boundary-layer dynamics. The near-zero global mean  $ERF_{ARI}$  results from the cancellation of  
487 positive and negative regional forcings. Positive mean  $ERF_{ARI}$  values (up to  $10 \text{ W m}^{-2}$ ) occur in regions where carbonaceous  
488 aerosols often overlie relatively high-albedo clouds (continental Asia and off the west coasts of Africa and South America).  
489 It is in these regions that the standard deviation of  $ERF_{ARI}$  is also largest (up to  $5 \text{ W m}^{-2}$ ). Light-absorbing aerosols above  
490 cloud heat the local atmosphere, which can suppress convection and affect cloud cover. This is important for calculating the  
491  $ERF_{ARI}$  from our simulations because we account for above-cloud scattering and absorption of aerosols in line with Ghan  
492 (2013). Neglecting the effects of above-cloud aerosols in the  $ERF_{ARI}$  produces no positive values for this forcing component  
493 (95% credible interval  $-0.69$  to  $-0.24$ ; Yoshioka et al., In prep.). Therefore, the magnitude of  $ERF_{ARI}$  over Asia, Africa and  
494 South America (where it is positive and reduces cloud cover) determines the sign of global mean  $ERF_{ARI}$ .  
495

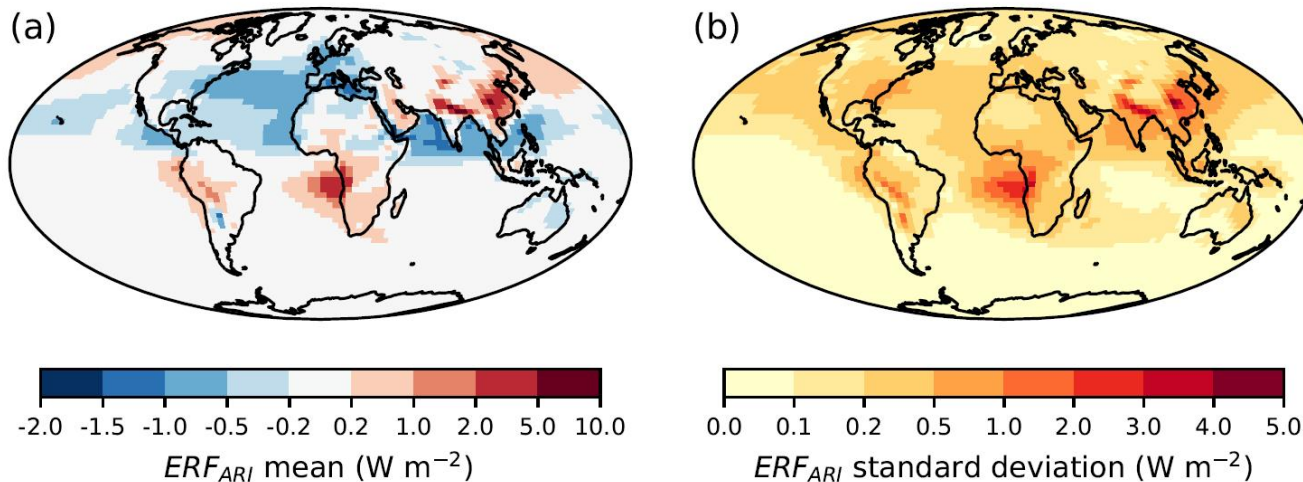


**Figure 3.** (a) Mean and (b) standard deviation of 1850-2008  $ERF_{ARI}$  forcing. Values were calculated using output from 270000 emulator-derived model variants at the individual pixel level. These samples of model variants are informed by the expert-elicited parameter pdfs.



## 496 3.2 Sources of uncertainty in aerosol ERF and its components

### 497 3.2.1 Sources of uncertainty in global mean $ERF_{ACI}$

498 Fig. 4 summarises the causes of variance (sometimes referred to as the ‘main effects’) in global mean  $ERF_{ACI}$ ,  $ERF_{ARI}$  and  
499 aerosol ERF. Natural aerosol emissions (here, Sea\_Spray, DMS and BB\_Diam) persist as important sources of industrial-period  
500  $ERF_{ACI}$  uncertainty, as in previous studies of several climate models (Wilcox et al., 2015) and the aerosol-only component of  
501 a global model (Carslaw et al., 2013). However, by far the largest source of uncertainty is the Rad\_Mcica\_Sigma parameter.  
502 This cloud radiation parameter affects the spatial homogeneity of simulated clouds, altering (amongst other things) reflected  
503 radiation, tropospheric temperature profiles and cloud amount. Therefore, by altering the radiative *state* of clouds in the pre-  
504 industrial and present-day atmospheres Rad\_Mcica\_Sigma affects uncertainty in the simulated *change* in cloud radiative state  
505 (the  $ERF_{ACI}$ ). Model process parameters Sig\_W and C\_R\_Correl cause uncertainty in  $ERF_{ACI}$  by altering the efficiency of  
506 the cloud droplet activation and deposition processes respectively. Other parameters cause a small amount of the  $ERF_{ACI}$   
507 uncertainty but only in individual months. Therefore, the six parameters and associated processes identified here are the key to  
508 understanding the uncertainty in the global, annual mean  $ERF_{ACI}$  in HadGEM.

509

### 510 3.2.2 Sources of uncertainty in global mean $ERF_{ARI}$

511 The sources of global mean  $ERF_{ARI}$  variance are summarised in Fig. 4(b). Parameters related to the emission and radiative  
512 properties of carbonaceous absorbing aerosols (BC\_RI, OC\_RI and BB\_Ems) are amongst the largest sources of  $ERF_{ARI}$   
513 variance in all months. However, the emission flux of carbonaceous aerosols (BB\_Ems) and the radiative properties of organic  
514 carbonaceous aerosols (OC\_RI) cause much more of the  $ERF_{ARI}$  variance in high emission months (Jun - Aug) than they do in  
515 the annual mean. In other months with lower concentrations of carbonaceous aerosols, uncertainty in anthropogenic emissions  
516 (here, Anth\_SO2) is the largest source of global mean  $ERF_{ARI}$  variance. Anthropogenic emissions affect the  $ERF_{ARI}$  by in-  
517 fluencing aerosol properties in the present-day atmosphere. Other parameters (notably, Rad\_Mcica\_Sigma and Sig\_W) affect  
518 the balance between  $ERF_{ACI}$  and  $ERF_{ARI}$  by altering cloud radiative properties which are important for calculating above-  
519 cloud aerosol effects (Ghan, 2013). Rad\_Mcica\_Sigma and Sig\_W are the only parameters identified as important causes of  
520 uncertainty in both  $ERF_{ACI}$  and  $ERF_{ARI}$ .

521

### 522 3.2.3 Sources of uncertainty in industrial-period global mean aerosol ERF

523 The aerosol ERF is the sum of the  $ERF_{ACI}$  and  $ERF_{ARI}$ . Therefore, the sources of aerosol ERF variance are also sources of  
524 variance in the forcing components. The causes of aerosol ERF variance are summarised in Fig. 4(c). Aerosol ERF shares more  
525 sources of variance with  $ERF_{ACI}$  than with  $ERF_{ARI}$  because  $ERF_{ACI}$  is the stronger and more uncertain forcing component  
526 (Fig. 1). Natural aerosol emissions (Sea\_Spray, DMS and BB\_Diam) and model process parameters (Sig\_W and C\_R\_Correl)

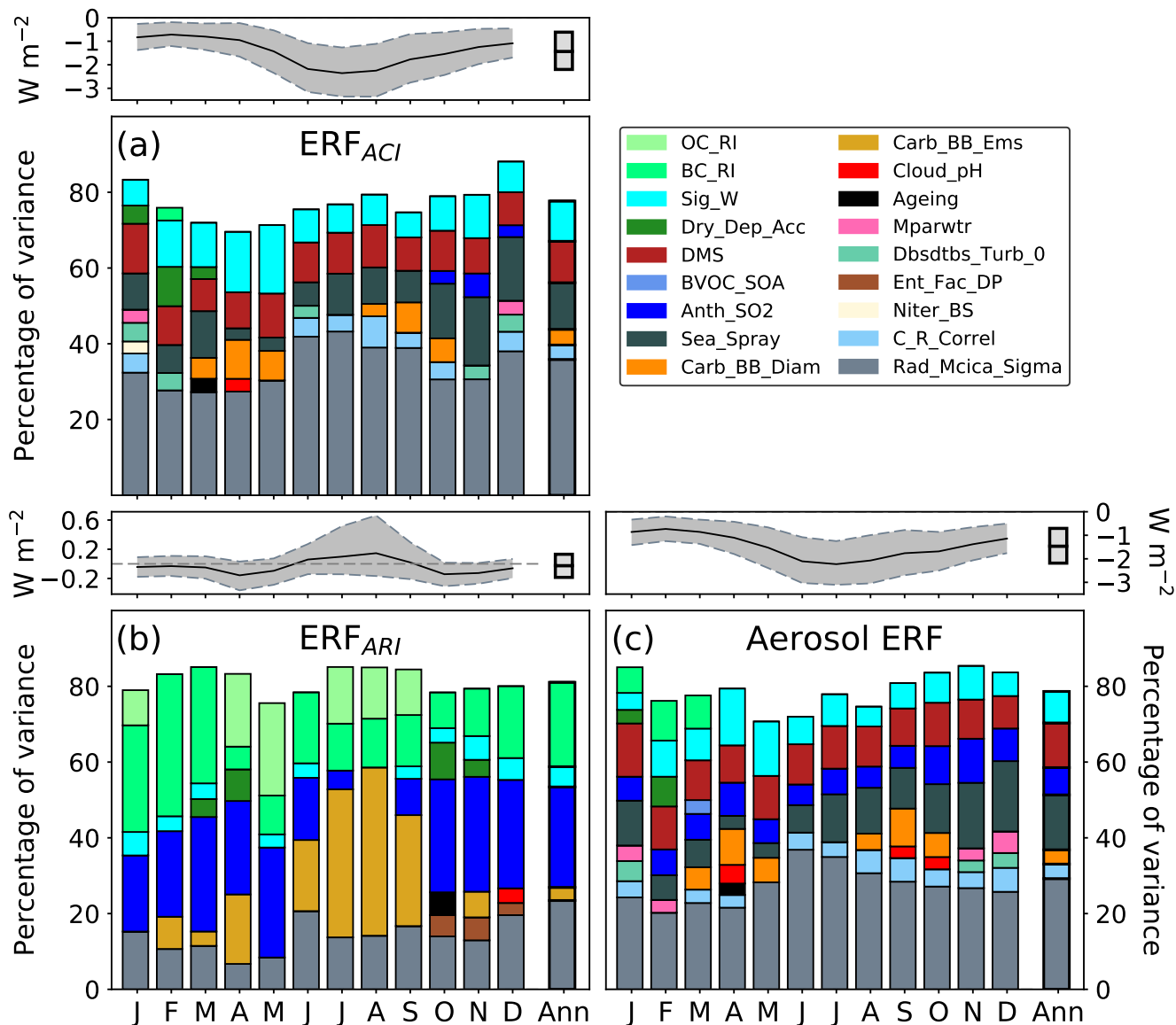


**Figure 4.** Percentage contributions to variance in global, monthly and annual mean 1850-2008 (a)  $ERF_{ACI}$ , (b)  $ERF_{ARI}$  and (c) aerosol ERF. Each bar contains only those parameters that cause at least 3% of the variance and interactions between parameters are neglected. Therefore, the percentage of variance accounted for is less than 100%. The monthly and annual median values and 95% credible intervals (from the 270000 model variants) are displayed in the top panel. The monthly median values are connected in bold and the credible intervals are shaded gray.

527 collectively cause over half of the aerosol ERF variance. Each of these key parameters causes a similar proportion of the  
 528 aerosol ERF and  $ERF_{ACI}$  variances. However, the cloud radiation parameter (Rad\_Mcica\_Sigma) causes more of the  $ERF_{ACI}$



529 variance (around 35%) than aerosol ERF variance (less than 30%), despite also causing around 25% of the  $ERF_{ARI}$  variance.  
530 This suggests that the  $ERF_{ACI}$  and  $ERF_{ARI}$  responses to  $Rad\_Mcica\_Sigma$  are of opposite sign and thus partially cancel in  
531 the aerosol ERF calculation. The other main difference between sources of aerosol ERF and  $ERF_{ACI}$  variance comes from  
532 anthropogenic emissions. Anthropogenic emission uncertainty ( $Anth\_SO2$ ) causes up to 10% of the aerosol ERF variance in  
533 all months. However,  $Anth\_SO2$  only causes a small percentage of the  $ERF_{ACI}$  variance in a few months. Therefore, this  
534 parameter's contribution to aerosol ERF variance is predominantly through its influence on the  $ERF_{ARI}$  component of forcing.  
535

### 536 3.2.4 Sources of uncertainty in multi-decadal aerosol ERF

537 The causes of aerosol radiative forcing uncertainty are known to depend on the anthropogenic emission period examined  
538 (Carslaw et al., 2013; Regayre et al., 2014). A more detailed understanding of the causes of uncertainty in aerosol ERF re-  
539 quires sensitivity analyses over multiple time periods. In this section, we examine the pattern of uncertainty in multi-decadal  
540 (1978-2008) aerosol ERF, identify the main causes of uncertainty in multi-decadal aerosol ERF and discuss how these results  
541 inform our understanding of aerosol ERF on longer time scales.

542

543 Fig. 5 shows the spatial pattern of mean aerosol ERF and its standard deviation over the 1978-2008 period. Global anthro-  
544 pogenic sulphate emissions peaked in the late 1970s (Lamarque et al., 2010) then decreased in Europe and North America as  
545 a result of clean air legislation, but increased significantly in Asia (Smith et al., 2011). Therefore, there are distinct regions  
546 of positive and negative aerosol ERF in the 1978-2008 period. The cancellation of the regional aerosol ERFs of opposite sign  
547 cause a near-zero global mean aerosol ERF (95% credible range of  $-0.6$  to  $0.8 \text{ W m}^{-2}$ ). Over continental land masses, the  
548 aerosol ERF standard deviation is largest (between  $0.5$  and  $5 \text{ W m}^{-2}$ ) in regions of substantial mean aerosol ERF (absolute  
549 mean larger than around  $1 \text{ W m}^{-2}$ ). The aerosol ERF standard deviation is larger than around  $0.3 \text{ W m}^{-2}$  over most marine  
550 regions and is largest over regions of persistent stratocumulus cloud, even when the mean forcing is near-zero (e.g. off the west  
551 coast of South America). This suggests the sign of recent-decadal aerosol ERF forcing is uncertain over those regions.

552

553 The sources of variance in aerosol ERF and its components over the 1978 to 2008 period are summarised in Fig. 6. The  
554 sign of the aerosol ERF over the 1978-2008 period is uncertain for much of the year and is only definitively negative in the  
555 Northern Hemisphere summer. The cancellation of positive and negative regional aerosol ERFs has three main implications  
556 for the global mean sensitivity analysis. Firstly, not all of the causes of regional aerosol ERF will be evident in the global mean  
557 analysis (Regayre et al., 2015). Nevertheless, the causes of uncertainty in global mean 1978-2008 aerosol ERF will inform  
558 our understanding. Secondly, the causes of global mean aerosol ERF uncertainty are seasonally dependent because changes in  
559 the magnitude of incoming solar radiation determine the relative importance of regional uncertainties. Thirdly, the competing  
560 regional effects cause the total variance accounted for by individual parameters to be much less than 100% (as low as 55% in  
561 some months) with many parameters causing only a small amount (around 5%) of the variance. This suggests that important  
562 interactions between multiple parameters in multiple regions are causing much of the global mean aerosol ERF variance in



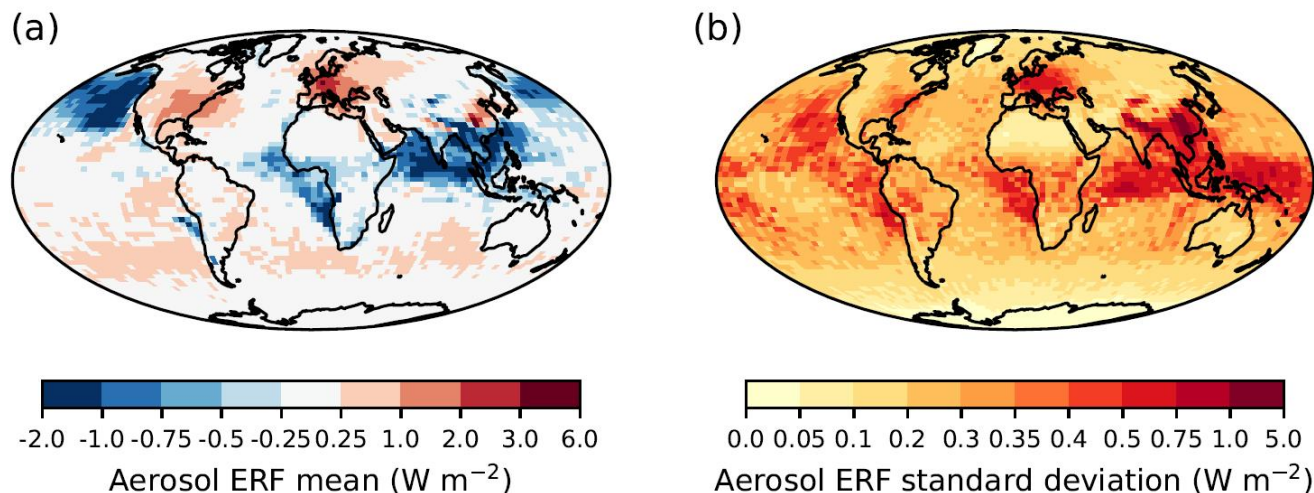


**Figure 5.** (a) Mean and (b) standard deviation of 1978-2008 aerosol ERF. Values were calculated using output from 270000 emulator-derived model variants at the individual pixel level. These samples of model variants are informed by the expert-elicited parameter pdfs.

563 recent decades.

564

565 There are multiple ways in which the causes of aerosol ERF uncertainty in the 1978-2008 period differ from those in the  
566 1850-2008 period. Firstly, natural aerosol emission parameters have little influence on recent-decadal aerosol ERF uncertainty  
567 because the global mean 1978-2008 aerosol ERF depends more linearly on changing anthropogenic emissions than the 1850-  
568 2008 aerosol ERF (Carslaw et al., 2013). Secondly, the cloud radiation parameter `Rad_Mcica_Sigma` causes very little (less  
569 than 3%) of the 1978-2008 aerosol ERF variance. The reduced importance of this parameter as a cause in aerosol ERF un-  
570 certainty results from the cancellation of regional aerosol ERFs of opposite sign, which also depends on the linearity of the  
571 multi-decadal aerosol ERF response to anthropogenic emission changes. Thirdly, in the 1978-2008 period anthropogenic and  
572 model process parameters are a larger source of aerosol forcing uncertainty, as in previous analysis of this period (Regayre  
573 et al., 2014). Here, uncertainty in the deposition rates of aerosols and aerosol precursor gases account for most (around 20%  
574 each) of the multi-decadal aerosol ERF variance. The aerosol process parameter `Cloud_pH` causes another 10% of the 1978-  
575 2008 aerosol ERF variance. The anthropogenic emission parameter `Anth_SO2` and other model process parameters (`Sig_W`,  
576 `Rain_Frac`, and `BC_RI`) each cause only a small amount (around 3%) of the variance.

577

### 578 3.3 Sources of uncertainty in ToA radiative flux

579 Identifying the sources of ToA reflected shortwave radiation (RSR) uncertainty will inform our understanding of how radiative  
580 flux measurements can help to constrain the aerosol ERF uncertainty (Lohmann and Ferrachat, 2010) because the aerosol ERF

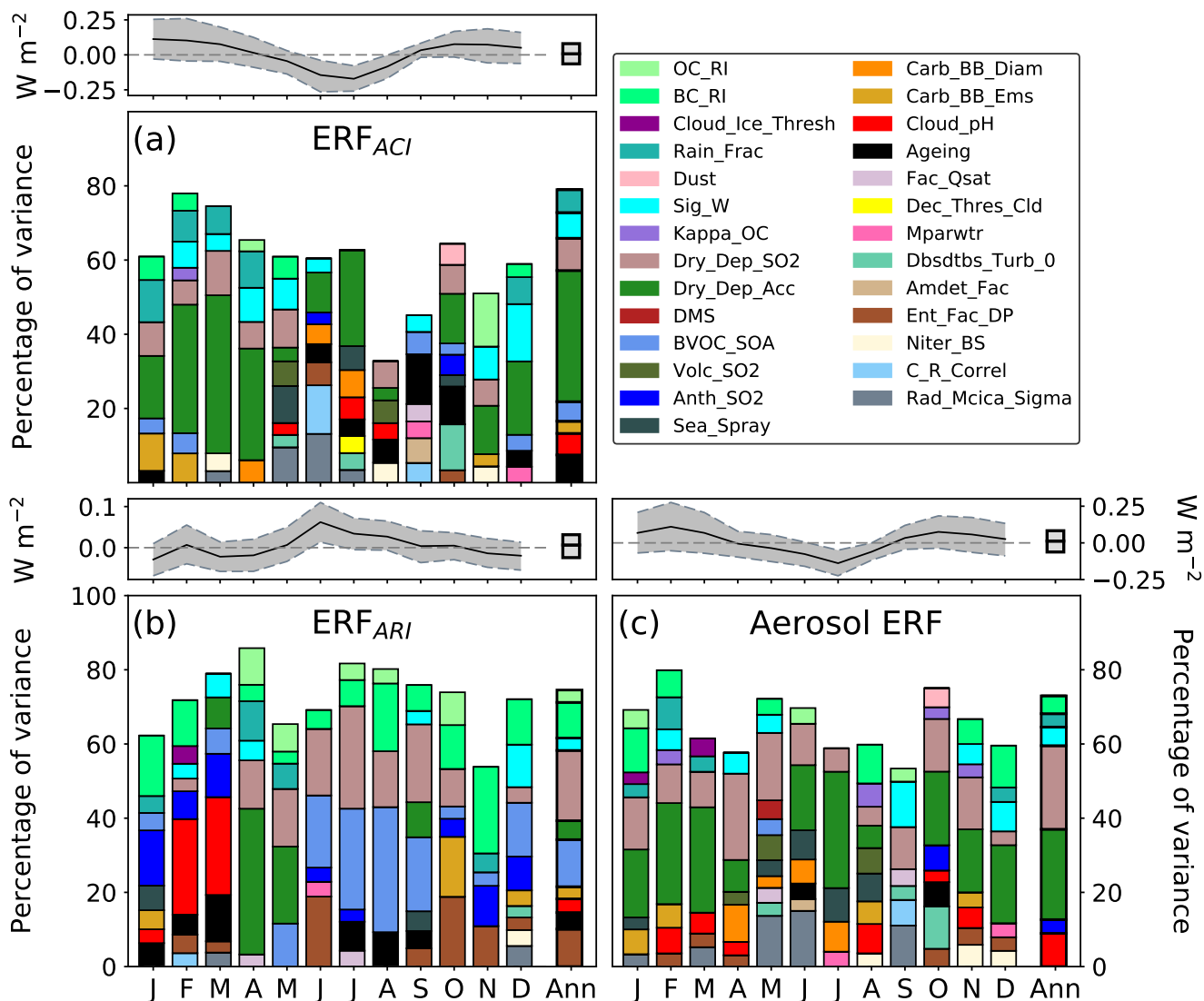


**Figure 6.** Percentage contributions to variance in 1978-2008 global, monthly and annual mean (a)  $ERF_{ACI}$ , (b)  $ERF_{ARI}$  and (c) aerosol ERF. Figure features are identical to Fig. 4.

581 is essentially the aerosol-forced change in RSR between the pre-industrial (or 1978) and present-day atmospheres (plus addi-  
 582 tional small changes in outgoing long-wave radiation). The causes of present-day ToA RSR variance are summarised in Fig. 7  
 583 and are very similar in the pre-industrial and 1978 atmospheres (not shown).

584

585 The dominant source of ToA RSR uncertainty is the cloud radiation parameter  $Rad\_Mcica\_Sigma$ , which was also the  
 586 dominant parameter for the pre-industrial to present-day aerosol ERF. Uncertainty in this parameter alone causes over 60% of

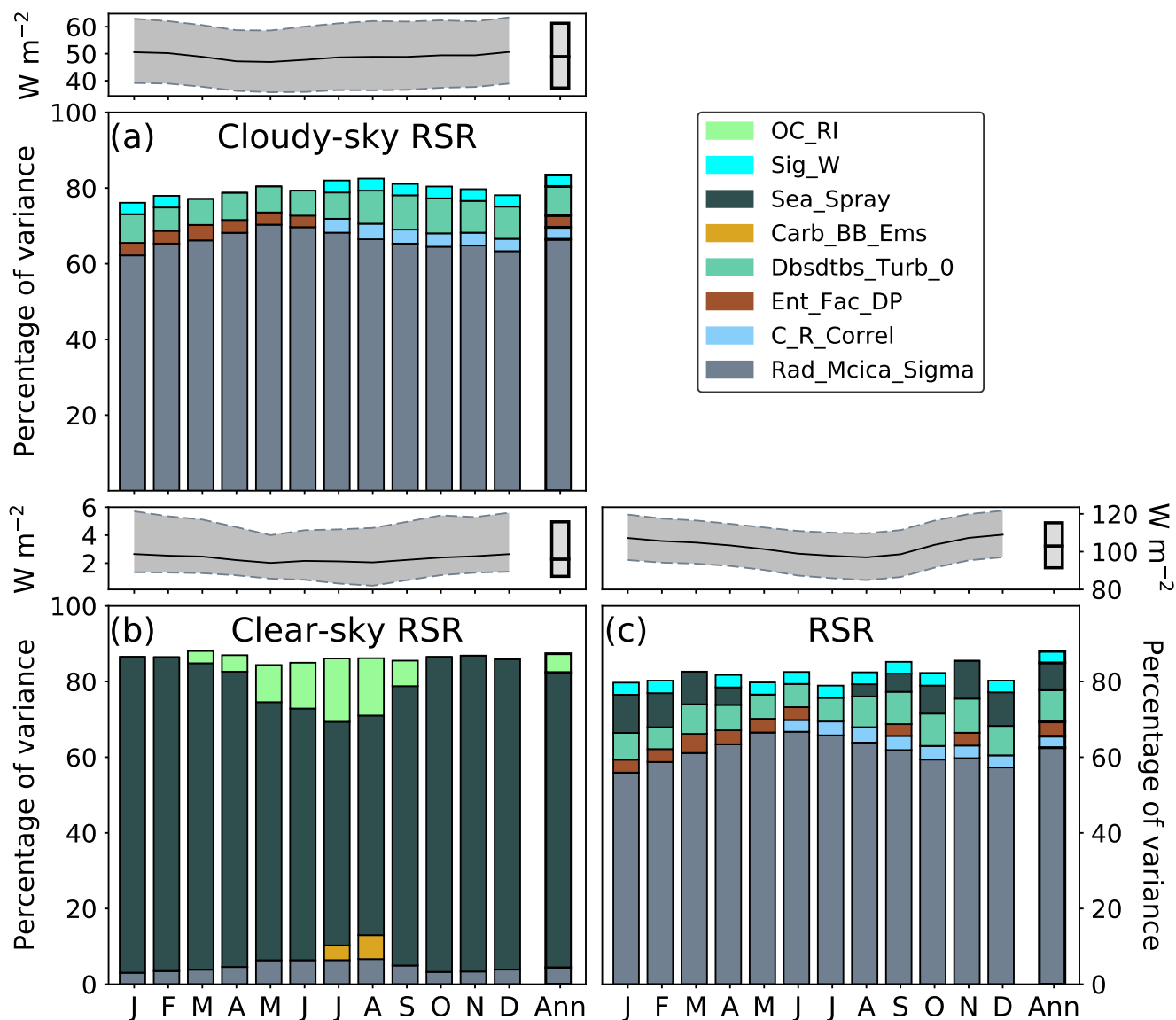


**Figure 7.** Percentage contributions to variance in present-day (2008) global, monthly and annual mean ToA (a) cloudy-sky RSR, (b) clear-sky RSR and (c) RSR. Figure features are identical to Fig. 4.

587 the RSR variance by altering the total cloud albedo. The dominant role of this cloud radiative parameter in causing uncertainty  
 588 in the ToA radiative flux and aerosol ERF suggests that constraining this parameter to a very narrow range should constrain the  
 589 uncertainty in radiative fluxes (Haerter et al., 2009; Lohmann and Ferrachat, 2010) and consequentially in aerosol ERF (Lee  
 590 et al., 2016). But of course, there are a number of other parameters (Dbsdtbs\_Turb\_0, Ent\_Fac\_DP, Sig\_W and C\_R\_Correl)  
 591 that cause ToA RSR uncertainty by altering the amount and/or albedo of clouds in the model. The mechanisms for altering



592 cloudiness and therefore the ToA radiative flux are different for each parameter. The Dbsdtbs\_Turb\_0 parameter causes around  
 593 10% of the ToA RSR variance by altering the mixing rate of clean and cloudy air masses. Increasing the proportion of dry  
 594 air in clouds has a dramatic effect on the amount of low-altitude cloud simulated in the model, making Dbsdtbs\_Turb\_0 the  
 595 dominant cause of uncertainty in low-altitude cloud-fraction (Fig. 8). The Ent\_Fac\_Dp, Sig\_W and C\_R\_Correl parameters  
 596 each cause around 5% of the RSR variance. The Ent\_Fac\_Dp parameter affects the strength of convection which also alters  
 597 precipitation rates and the vertical distribution of simulated clouds. Sig\_W controls the activation of cloud condensation nuclei  
 598 into cloud droplets (affecting droplet effective radius and cloud albedo) and C\_R\_Correl alters the rate of cloud droplet accre-  
 599 tion by precipitating rain drops. The only parameter to cause ToA RSR variance (around 10%) by directly altering atmospheric  
 600 aerosol concentrations is Sea\_Spray.

601

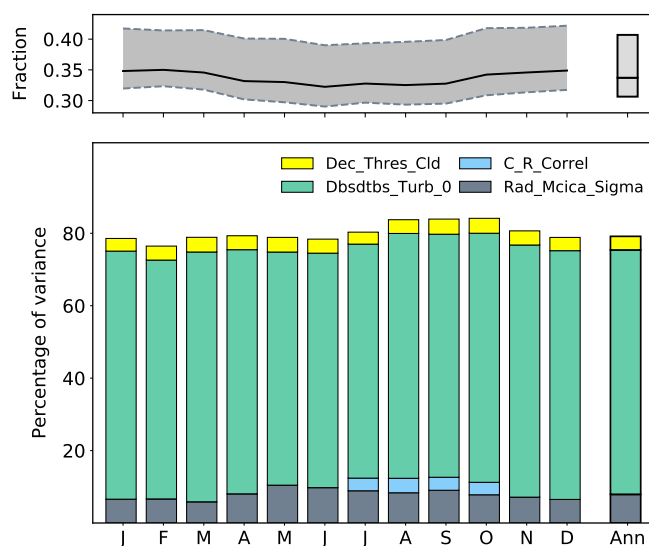


**Figure 8.** Percentage contributions to variance in present-day (2008) global, monthly and annual mean low altitude cloud amount. Figure features are identical to Fig. 4.

602 Figure 9 summarises the relative contributions of atmospheric and aerosol parameters to uncertainty in global mean values  
 603 of present-day ToA RSR (from Fig. 7) and aerosol ERFs over the periods 1978-2008 (Fig. 6) and 1850-2008 (Fig. 4). Atmo-  
 604 spheric parameters cause the majority (around 80%) of the variance in present-day ToA radiative flux, but only around 30%  
 605 of the variance in 1850-PD aerosol ERF, and less than 10% of the 1978-PD aerosol ERF variance. The rest of the uncertainty  
 606 is attributable to the aerosol model. This disparity arises because contributions to variance in aerosol ERF depend on how  
 607 parameters influence the atmosphere's response to the *change* in anthropogenic emissions, while RSR variance depends on  
 608 how they influence the *state* of the atmosphere.

609

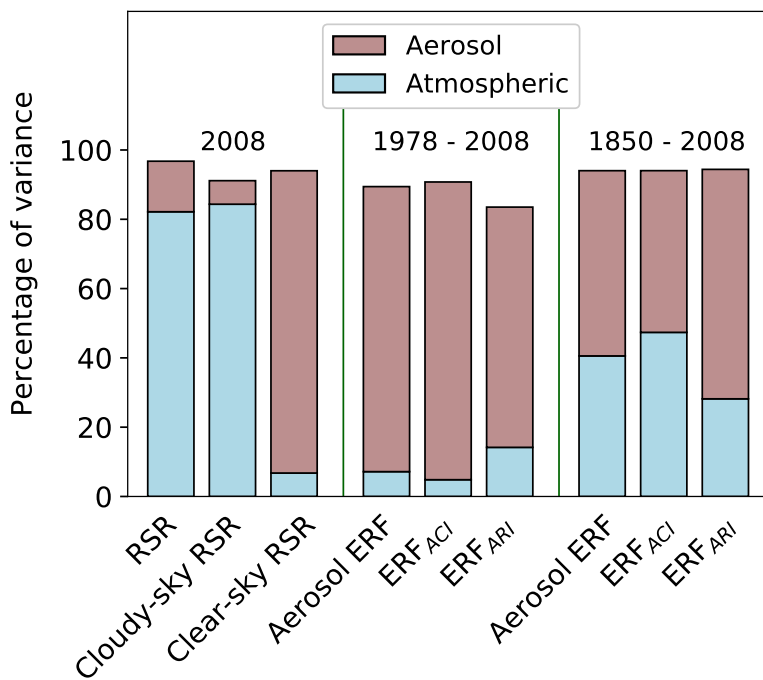


**Figure 9.** The relative contributions from atmospheric and aerosol parameters to variance in ToA radiative fluxes and aerosol effective radiative forcing over the 1978-2008 and 1850-2008 periods.

### 610 3.4 Identifying the sources of uncertainty at the regional level

#### 611 3.4.1 Regional sources of uncertainty

612 Regional forcings can be important drivers of global and regional climate change (Chalmers et al., 2012; Booth et al., 2012;  
613 Bollasina et al., 2013; Shindell et al., 2013; Kirtman et al., 2013; Villarini and Vecchi, 2013; Allen et al., 2014). Further-  
614 more, important sources of aerosol forcing uncertainty may be overlooked if regional sensitivity analysis results are neglected  
615 (Regayre et al., 2015). Examining how these sources of regional forcing uncertainty combine to cause uncertainty in global  
616 mean forcing uncertainty will inform our understanding of how to best observationally constrain the uncertainty. We identified  
617 regions of substantial aerosol ERF (stronger than around  $-2.5 \text{ W m}^{-2}$ ) for more in-depth analysis (Table A3 and Fig. 10). The  
618 corresponding sources of aerosol ERF variance in each region are summarised in Fig. 11.

619

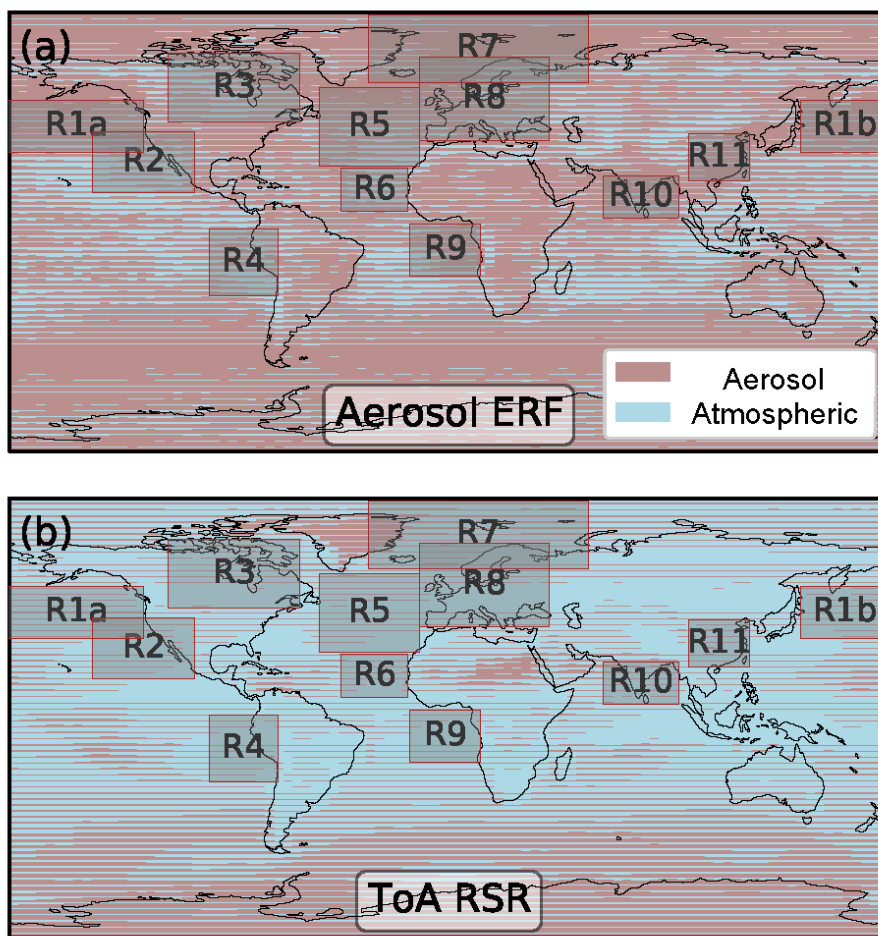


**Figure 10.** Maps of contributions to variance in (a) 1850-2008 aerosol ERF and (b) present-day (2008) ToA RSR from atmospheric and aerosol parameters. Each pixel contains a box that is shaded in proportion to the amount of variance caused by each source of uncertainty.



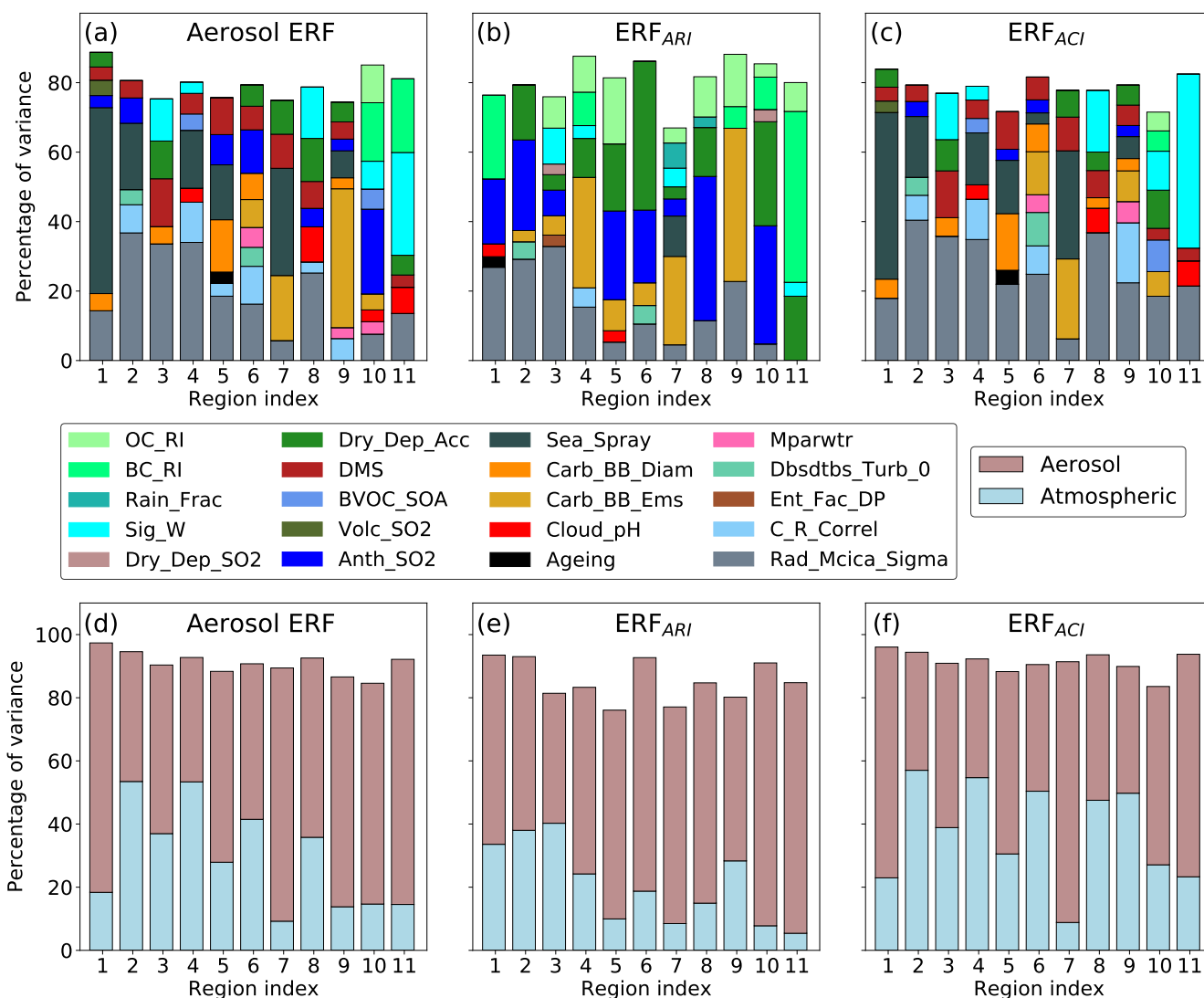


**Figure 11.** Sources of variance ((a), (b) and (c)) and grouped atmospheric and aerosol contributions to variance ((d), (e) and (f)) for 1850-2008 annual mean (a),(d) aerosol ERF, (b),(e)  $ERF_{ARI}$  and (c),(f)  $ERF_{ACI}$  for the 11 regions defined in table A3 and highlighted in Fig. 10.

620 The main causes of regional aerosol ERF uncertainty are often those parameters that cause global mean uncertainty. How-  
 621 ever, there are substantial differences between regions. Some parameters are important causes of global mean aerosol ERF  
 622 uncertainty because they cause a small amount (at least 5%) of the uncertainty in nearly all regions. For example, the DMS  
 623 parameter causes around 5% of the aerosol ERF variance in most regions and consequentially causes around 15% of the global  
 624 mean variance. The cloud radiation parameter Rad\_Mcica\_Sigma (which causes nearly 30% of the industrial-period aerosol  
 625 ERF variance) also causes aerosol ERF variance in most regions. But, the amount of regional aerosol ERF variance accounted



626 for by this parameter ranges from less than 3% (R9) to around 35% (R2, R3, R4).

627

628 Other parameters are important causes of global mean aerosol ERF uncertainty despite being important causes of uncertainty  
629 in only around half of the regions examined. For example, the Sea\_Spray parameter (which causes nearly 20% of the global  
630 mean aerosol ERF variance) is by far the largest source (around 60%) of aerosol ERF variance in the North Pacific (R1) and  
631 causes between 10 and 30% of the variance in several other marine regions. However, in tropical marine regions (R6 and R10)  
632 and regions containing continental land mass (R3, R8 and R11) Sea\_Spray causes less than 3% of the aerosol ERF variance.  
633 The land-based regions (R3, R8, R11) are also where the cloud updraft parameter Sig\_W causes aerosol ERF variance. The  
634 importance of Sig\_W over continents suggests cloud albedo is most sensitive to uncertainty in updraft velocity in the most-  
635 polluted regions where cloud droplet concentrations are updraft-limited (Reutter et al., 2009; Sullivan et al., 2016).

636

637 Anth\_SO2 makes its greatest contribution to aerosol ERF uncertainty in tropical marine regions (R6 and R10) by causing  
638 uncertainty in  $ERF_{ARI}$ . The Anth\_SO2 parameter also causes up to 40% of the  $ERF_{ARI}$  variance near anthropogenic sources  
639 (R3 and R8) and up to 30% in outflow regions (R1, R2, R5). However, these substantial causes of  $ERF_{ARI}$  variance translate  
640 into small (less than 10%) causes of aerosol ERF variance in most regions. The aerosol deposition parameter (Dry\_Dep\_Acc)  
641 also causes more of the regional  $ERF_{ARI}$  variance (up to 45%) than regional aerosol ERF variance (less than 15%). However,  
642 despite being an important cause of 1850-2008 aerosol ERF uncertainty in several regions, the dry deposition parameter is not  
643 an important cause of global mean aerosol ERF uncertainty over this period (Fig. 4(c)).

644

645 The importance of carbonaceous aerosol parameters (Carb\_BB\_Ems, Carb\_BB\_Diam, BC\_RI and OC\_RI) as causes of  
646 aerosol ERF uncertainty are highly region dependent. Uncertainty in the emission flux of carbonaceous aerosols Carb\_BB\_Ems  
647 causes between 25 and 45% of the  $ERF_{ARI}$  variance in and near biomass burning regions (R4, R7 and R9). However, this only  
648 translates into a cause of aerosol ERF uncertainty in regions R7 and R9 where the Carb\_BB\_Ems parameter also causes uncer-  
649 tainty in  $ERF_{ACI}$ . Uncertainty in the size of emitted carbonaceous absorbing aerosols (Carb\_BB\_Diam) is more important as  
650 a cause of uncertainty in  $ERF_{ACI}$  than in  $ERF_{ARI}$  because it determines the capacity for carbonaceous aerosols to act as cloud  
651 condensation nuclei. Therefore, Carb\_BB\_Diam predominantly causes aerosol ERF variance (up to 15%) in the cloudiest  
652 regions (R1, R5, R6 and R9). Uncertainty in the radiative properties of carbonaceous aerosols (BC\_RI and OC\_RI) collec-  
653 tively cause  $ERF_{ARI}$  variance in almost all regions. However, uncertainty in aerosol ERF is affected by these parameters only  
654 over China (R11) and near to India (R10). Over China the anthropogenic emission parameter (Anth\_SO2) is surpassed by the  
655 BC\_RI and OC\_RI parameters as causes of  $ERF_{ARI}$  and aerosol ERF uncertainty, despite carbonaceous aerosols making up  
656 a relatively small proportion of aerosol emissions in these regions (Granier et al., 2011). The BC\_RI parameter causes around  
657 50% of the  $ERF_{ARI}$  variance and around 25% of the variance in aerosol ERF in China. However, anthropogenic emissions  
658 do cause uncertainty in  $ERF_{ARI}$  and aerosol ERF in the Pacific (an outflow region for Chinese emissions). Near India, uncer-  
659 tainty in BC\_RI and OC\_RI cause around 30% and 10% of the aerosol ERF variance respectively and cause a smaller amount  
660 (between 5 and 10%) of variance in each of the forcing components. Despite being important sources of forcing uncertainty at



661 the regional level, Carb\_BB\_Diam is the only parameter related to carbonaceous aerosols which causes uncertainty in global,  
662 annual mean aerosol ERF.

663

664 Figure 11 (d)-(f) shows that atmospheric parameters combined can cause up to around 50% of the regional aerosol ERF vari-  
665 ance despite causing only around 30% of the global mean aerosol ERF variance. However, there are multiple regions where  
666 uncertainty in the physical atmosphere parameters causes less than 20% of the aerosol ERF variance. Where atmospheric pa-  
667 rameters are an important source of regional aerosol ERF uncertainty, the Rad\_Mcica\_Sigma parameter is almost always the  
668 most important. On its own uncertainty in Rad\_Mcica\_Sigma causes over 20% of the aerosol ERF variance in coastal Pacific  
669 regions (R2 and R4) as well as continental regions (R3 and R8). The atmospheric parameter controlling the accretion rate  
670 of aerosols by rain drops (C\_R\_Correl) causes around 10% of the aerosol ERF variance in several tropical or sub-tropical  
671 regions off the western coast of continents (R2, R4, R6 and R9). These are all regions of persistent stratocumulus cloud where  
672 cloud albedo is highly susceptible to changes in aerosol concentrations and size distributions. The clear- and cloudy- air mix-  
673 ing parameter Dbsdtbs\_Turb\_0 causes between 5 to 10% of the variance in aerosol ERF and its components in the Northern  
674 Hemisphere regions of persistent stratocumulus cloud (R2 and R6) but not in Southern Hemisphere regions (R4 and R9). This  
675 suggests that the relatively polluted Northern Hemisphere stratocumulus clouds are more sensitive to the sub-grid mixing of  
676 clear- and cloudy air masses. In tropical regions (R6, R9 and R10) the convective parameter Mparwtr causes a small amount  
677 (3 to 5%) of the aerosol ERF variance. This parameter alters the timing of precipitation and therefore affects cloud and aerosol  
678 amount, and the  $ERF_{ACI}$  near the equator where convective instability and precipitation are greatest. The regions where phys-  
679 ical atmosphere parameters cause the least aerosol ERF variance are either near to anthropogenic emission sources (R9, R10  
680 and R11) or downwind of them (R1 and R7).

681

682 These results show that the relative importance of individual parameters as sources of uncertainty differ between regions.  
683 However, the most important causes of global mean aerosol ERF uncertainty also cause uncertainty at the regional level.

684

### 685 3.5 Observational constraint of the aerosol ERF uncertainty

#### 686 3.5.1 Effect of ToA RSR constraint on aerosol ERF uncertainty

687 We now explore the extent to which present-day measurements of global mean ToA RSR could in principle help to constrain  
688 the change in flux between two time periods (the aerosol ERF), which was previously explored by Lohmann and Ferrachat  
689 (2010) who perturbed four physical atmosphere parameters. We expect some constraint of aerosol ERF uncertainty based on  
690 the common causes of uncertainty in ToA RSR and aerosol ERF. Observational constraint of a model output variable can lead  
691 to constraint of the uncertain parameters. Therefore, when two model output variables share common causes of uncertainty  
692 we can expect that constraint of one output will lead to constraint of the other. Our approach of drawing large samples of one  
693 million parameter combinations from model emulators (using uniform pdfs for each parameter; Section 2.3) enables this link



694 through the uncertain parameters to be understood, which is not possible just from a perturbed parameter ensemble alone (e.g.  
695 Lohmann and Ferrachat, 2010).

696

697 Our analysis reveals substantial overlap in the combinations of parameters causing uncertainty in 1850-2008 aerosol ERF  
698 and present-day ToA RSR. The parameters Rad\_Mcica\_Sigma, Sea\_Spray, C\_R\_Correl and Sig\_W account for about 60%  
699 of the aerosol ERF uncertainty and about 80% of the ToA flux uncertainty. It is important to note that it is irrelevant for  
700 the observational constraint process that the ToA flux is much larger than the aerosol ERF. The important factor is that their  
701 uncertainties are caused by common uncertain parameters, so constraint of one of them will constrain the other through the  
702 constraint of the plausible parameter ranges and relationships.

703

704 Figure 12 shows the effect of constraining the modelled present-day RSR to within  $\pm 0.25 \text{ W m}^{-2}$  of  $98.3 \text{ W m}^{-2}$ , the  
705 multi-year average of observations from the Clouds and the Earth's Radiant Energy System (CERES; Loeb et al., 2009). The  
706  $\pm 0.25 \text{ W m}^{-2}$  represents within-CERES product uncertainty (Loeb et al., 2012) and neglects multiple other sources of satellite  
707 observational uncertainty (Loeb et al., 2009; Hartmann et al., 2013). We also neglect uncertainty caused by unknown model  
708 structural errors (Goldstein and Rougier, 2004; Sexton et al., 2012; Stier et al., 2013), observation representativeness errors  
709 (Schutgens et al., 2017) and the emulators themselves (Oakley and O'Hagan, 2004). Therefore, our RSR observational con-  
710 straint provides an upper bound on the potential reduction in aerosol ERF uncertainty. This tight constraint eliminates 97% of  
711 the model variants and the observationally constrained RSR range is less than 2% of the original unconstrained range. Conse-  
712 quently, the smaller set of model variants also predicts reasonably constrained 1978 and 1850 RSR ranges. However, despite  
713 reducing the plausible parameter space by 97% and the RSR range by 98% the impact on the aerosol ERF uncertainty is more  
714 modest. The effect of applying the RSR observational constraint is to rule out 1850-2008 aerosol ERF values lower than around  
715  $-2.4 \text{ W m}^{-2}$ , which represents around 15% of the original aerosol ERF range (the 95% credible range is reduced by around  
716 10%; Table A4). This reduction in aerosol ERF range is much less than the 56% reduction found by Lohmann and Ferrachat  
717 (2010) based on a set of 169 perturbed parameter simulations (compared to our one million model variants). We discuss the  
718 reasons for this modest reduction in aerosol ERF uncertainty in sections 3.5.2 and 3.5.3.

719

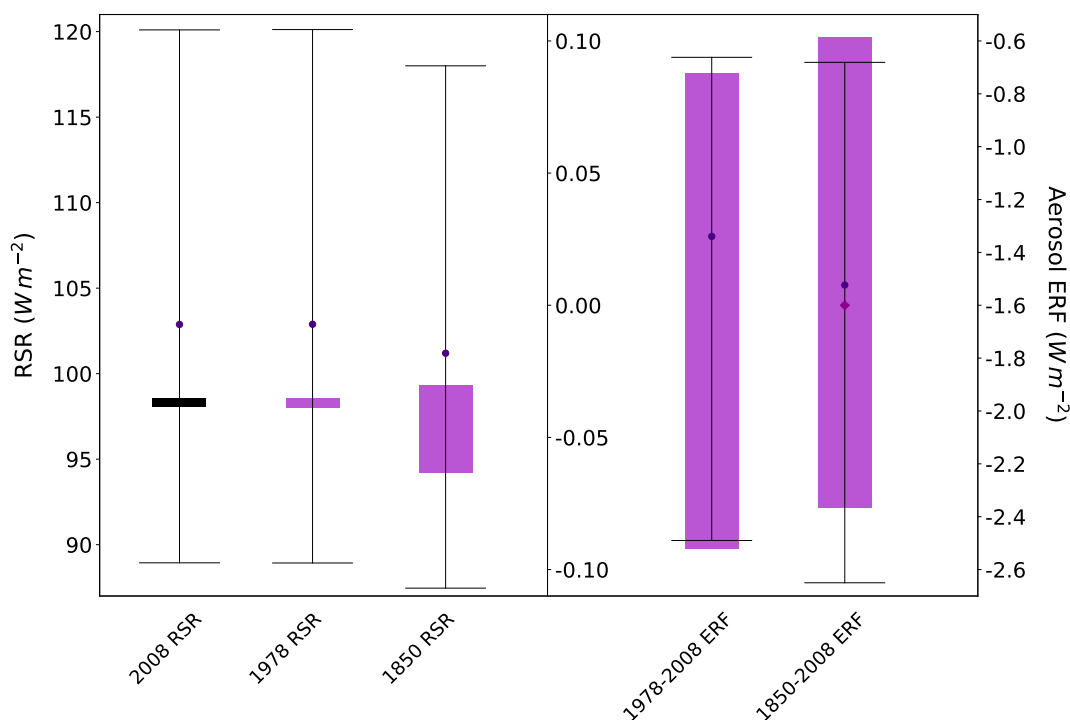


**Figure 12.** Observationally constrained present-day ToA RSR and the values of 1978 and 1850 ToA RSR and 1978-2008 and 1850-2008 aerosol ERF values from matching model variants. For each output variable the black lines show 95% credible intervals of the unconstrained one million member sample of model variants. The black box contains all model variants within  $\pm 0.25 W m^{-2}$  of the CERES-observed global annual mean present-day ToA RSR value. Purple boxes represent the 95% credible intervals of values obtained using model variants (parameter combinations) in the observationally constrained sample. The middle and right-hand axes are for 1978-2008 and 1850-2008 aerosol ERF respectively. Output from the simulation with all parameters set to their median values are shown as dots. The median 1850-2008 aerosol ERF from the observationally constrained sample is displayed as a diamond.

### 720 3.5.2 Constraining the relationships between the aerosol ERF and uncertain parameters

721 Fig. 13 shows how aerosol ERF is related to the values of the four main causes of aerosol ERF uncertainty before and after  
722 applying the observational constraint. There are clear relationships between the aerosol ERF and the individual parameters,  
723 but they are highly uncertain (even in the constrained sample) because there are many compensating errors among the other  
724 parameters (i.e., many ways to combine the parameters to get the same ToA RSR but very different aerosol ERF; (Fig. 12)).  
725 This diversity of credible model variants would be overlooked had we perturbed parameters individually, as is the case with  
726 one-at-a-time perturbation experiments (e.g. Gettleman, 2015).

727

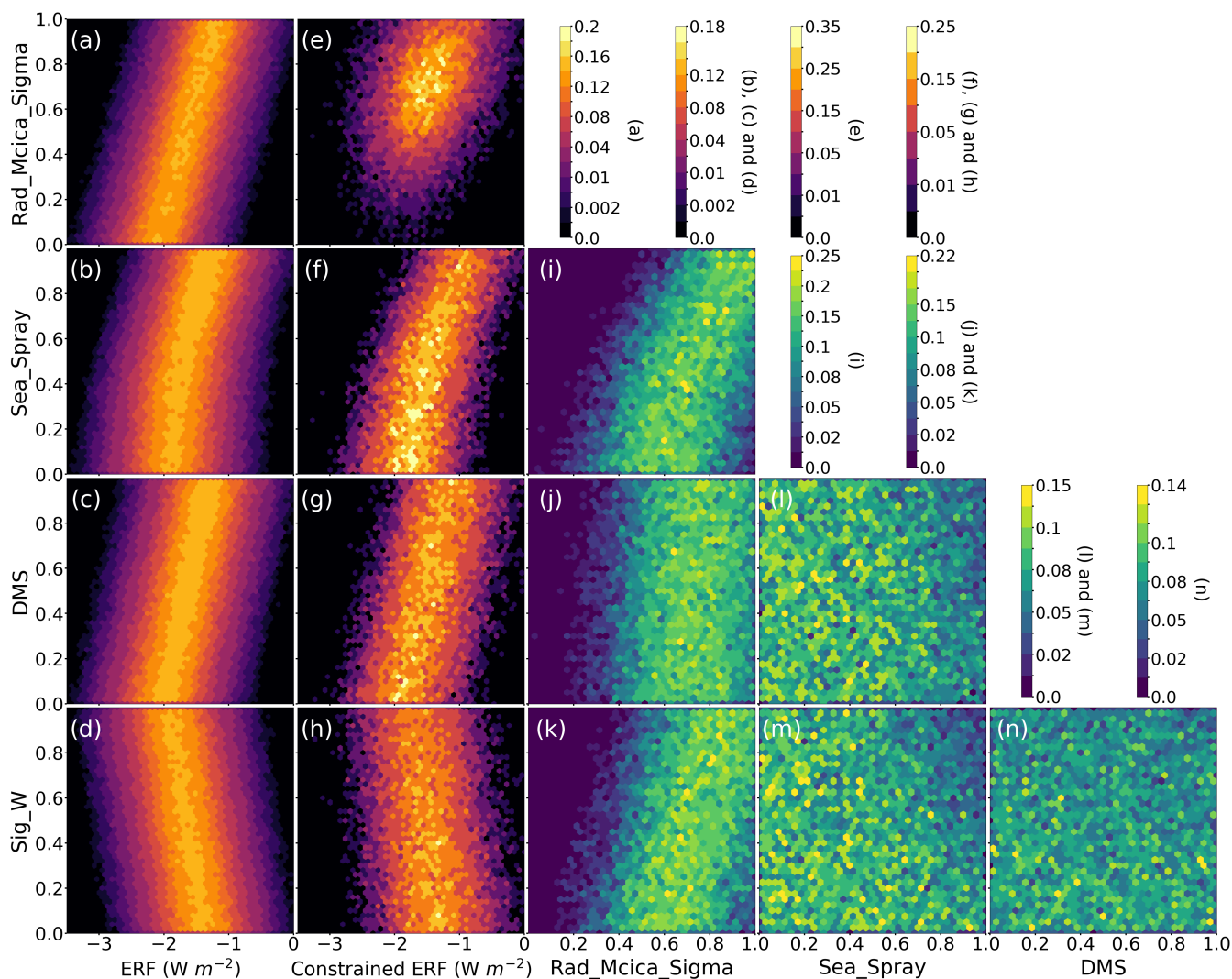


**Figure 13.** Probability density distributions of aerosol ERF and the parameters Rad\_Mcica\_Sigma, Sea\_Spray, DMS, Sig\_W in the unconstrained sample (first column; (a)-(d)) and in the sample constrained to match the observed global annual mean RSR (second column; (e)-(h)). Probability density distributions of parameter values are shown for the constrained sample ((i)-(n)). Colour bars labelled (a)-(n) correspond with the sub-figures and show the percentage of each sample within each pixel. Some colour bars apply to multiple panels.

728 For each of the one million model variants in our unconstrained sample individual parameter values were drawn from uni-  
 729 form distributions with ranges defined by the expert elicited pdfs. Therefore, prior to applying the observational constraint the  
 730 model variants were evenly dispersed across every two-dimensional parameter subspace. We are therefore able to quantify the  
 731 effect of the observational constraint on the plausibility of individual and combined parameter values.

732





733 The cloud radiation parameter  $\text{Rad\_Mcica\_Sigma}$  is negatively correlated with the ToA radiative flux and this leads to a pos-  
734 itive correlation with aerosol ERF: Increasing its value decreases the simulated cloud albedo and hence the ToA RSR. But, ToA  
735 RSR is more sensitive to  $\text{Rad\_Mcica\_Sigma}$  in the present-day atmosphere than in the pre-industrial (because higher aerosol  
736 concentrations increase the cloud albedo), so increasing the parameter value weakens the aerosol ERF. Figure 13 shows that  
737 low values of  $\text{Rad\_Mcica\_Sigma}$  (less than around 0.4 in the scaled range 0 to 1) are inconsistent with the observed RSR. The  
738 proportion of model variants with  $\text{Rad\_Mcica\_Sigma}$  values less than 0.4 drops from 40% in the unconstrained sample to just  
739 8% in the constrained case. In other words, the observational constraint suggests the plausible lower limit of this parameter is  
740 higher than we assumed in our expert elicitation. We can therefore state that the strongest aerosol ERFs are also implausible  
741 (as shown in Fig. 12) because they are associated with low values of  $\text{Rad\_Mcica\_Sigma}$ .

742

743 Figure 13 also shows that the aerosol ERF is weaker for larger  $\text{Sea\_Spray}$  and DMS values. An abundance of natural  
744 aerosols increases background (pre-industrial) atmospheric aerosol concentrations and limits the influence of anthropogenic  
745 aerosol emissions on clouds and radiation (Carslaw et al., 2013). Figure 13 shows that the observed ToA radiative flux is more  
746 consistent with low emissions of natural aerosols (the density of  $\text{Sea\_Spray}$  values larger than 0.5 decreases from 50% to  
747 44% after constraint of the ToA flux). The decreased likelihood of higher natural aerosol emissions in the constrained sample  
748 suggests that the weakest aerosol ERF values are less congruent with observed ToA RSR. However, there remain many obser-  
749 vationally plausible model variants with high natural aerosol emissions.

750

751 The largest values of the cloud updraft parameter ( $\text{Sig\_W}$ ) are also less plausible in the constrained sample (Fig. 13; 27%  
752 of the sample are larger than 0.7, instead of 30%). This suggests that present-day RSR observations are more consistent with  
753 lower vertical velocities, but the largest values cannot be ruled out completely because of the way that other compensating  
754 parameters affect RSR. Lower values of  $\text{Sig\_W}$  weaken the aerosol ERF by reducing cloud droplet concentrations primarily in  
755 the present-day polluted atmosphere, because cloud droplet activation is more sensitive to  $\text{Sig\_W}$  in the present-day atmosphere  
756 than in the aerosol-limited pre-industrial atmosphere. Therefore, observational constraint of ToA radiative flux reduces the  
757 likelihood of weak aerosol ERFs through a constraint of the distribution of  $\text{Sig\_W}$  values.

758

### 759 3.5.3 Constraining the relationships between uncertain parameters

760 Fig. 13 also shows the important parameter inter-dependencies revealed by observationally constraining the ToA radiative flux.  
761 The  $\text{Rad\_Mcica\_Sigma}$  and  $\text{Sea\_Spray}$  parameters are positively correlated in the observationally constrained sample. For  
762 example, a modelled ToA RSR consistent with observations can be achieved using high values of  $\text{Rad\_Mcica\_Sigma}$  (which  
763 decreases cloud albedo) and relatively high values of  $\text{Sea\_Spray}$  (which increases cloud albedo). In other words, these param-  
764 eters have compensating effects on the ToA radiative flux. The same compensation applies to the aerosol ERF: the weakest  
765 ERFs in our pdf (larger than around  $-1 \text{ W m}^{-2}$ ) are associated with high  $\text{Rad\_Mcica\_Sigma}$  and high  $\text{Sea\_Spray}$  values. How-  
766 ever, the RSR and aerosol ERF depend on these two parameters in quite different ways. Higher  $\text{Rad\_Mcica\_Sigma}$  values



767 *weaken* the aerosol ERF by *reducing* the present-day ToA RSR, whilst higher Sea\_Spray values *weaken* the aerosol ERF by  
768 *increasing* present-day RSR. Hence, constraining the relationship between the two largest sources of aerosol ERF uncertainty  
769 using observations of present-day RSR has not drastically reduced the aerosol ERF uncertainty.

770

771 The cloud droplet activation parameter (Sig\_W) is also positively correlated with Rad\_Mcica\_Sigma in the observationally  
772 constrained sample (Fig. 13). As with sea spray emissions, higher values of Sig\_W increase cloud albedo and compensate  
773 for the effect of high Rad\_Mcica\_Sigma values on ToA RSR. These parameters both exert a greater influence on present-  
774 day cloud radiative properties; in the case of Sig\_W, cloud radiative properties are more susceptible to this parameter in the  
775 present-day simulations because cloud droplet activation is more likely to be updraft-limited (rather than aerosol-limited) in  
776 an anthropogenically-polluted atmosphere. Therefore, in contrast to the Sea\_Spray and Rad\_Mcica\_Sigma relationship, the  
777 Sig\_W and Rad\_Mcica\_Sigma parameters have additive (not compensating) effects on aerosol ERF. Parameters with additive  
778 effects on the aerosol ERF are more susceptible to the effects of model equifinality. Therefore, the relationship between aerosol  
779 ERF and Sea\_Spray is better constrained than the relationship between aerosol ERF and Sig\_W.

780

781 The Sig\_W and Sea\_Spray parameters both act to counter the effect of Rad\_Mcica\_Sigma on cloud albedo in the con-  
782 strained sample. Therefore, the density of model variants with simultaneously large (above around 0.6) Sig\_W and Sea\_Spray  
783 values is lower in the constrained sample (down from 16% to 11%). No such restrictions apply to simultaneously small values  
784 (less than 0.4) of these two parameters. In fact the proportion of simultaneously small Sig\_W and Sea\_Spray in the sample  
785 increases from 16% to 19% after applying the constraint which rules out other parts of parameter space. This suggests that in  
786 simulations with low natural aerosol emissions and low cloud droplet activation efficiency, there are multiple other contributing  
787 factors keeping the ToA RSR in agreement with observations. For example, by limiting the mixing rates of clear and cloudy air  
788 masses, a low value of the Dbsdtbs\_Turb\_0 parameter (an important source of ToA RSR uncertainty) can compensate for the  
789 decrease in cloud droplet concentrations caused by a low value of the cloud droplet activation parameter. A replacement source  
790 of aerosols large enough to act as cloud condensation nuclei is also required to compensate for low natural aerosol emissions.  
791 There are multiple ways in which this could be achieved. For example, a low value of the dry deposition velocity parameter  
792 Dry\_Dep\_Acc (known to be important for cloud active aerosol concentrations; Lee et al., 2013) increases the atmospheric  
793 lifetime of aerosols, allowing them to grow in size and activate to form cloud droplets, even in a low activation efficiency  
794 simulations.

795

796 The DMS parameter has no obvious relationships with the other main sources of aerosol ERF uncertainty in the constrained  
797 sample. This is despite DMS affecting aerosol ERF in the same regions as other key parameters and causing aerosol ERF  
798 uncertainty through a similar mechanism to Sea\_Spray. In other words, higher values of DMS and Sea\_Spray suppress the  
799 aerosol ERF by increasing background (1850) aerosol concentrations. Therefore, the value of the DMS parameter is more  
800 likely (54% of the time) to be small (lower than 0.5) when the value of Sea\_Spray is high (above 0.8). In summary, model  
801 variants with high values of both of the important natural aerosol emission parameters are less likely to be consistent with the



802 observed ToA RSR.

803

804 These results highlight the importance of understanding the potential causes of equifinality when interpreting results from  
805 such a complex model (Beven and Freer, 2001). Reducing the remaining uncertainty in global mean aerosol ERF will require  
806 observations which further constrain the relationships between aerosol ERF and the key sources of uncertainty.

807

### 808 3.5.4 Regional constraint of global mean aerosol ERF uncertainty

809 Our overall aim is to constrain the uncertainty in global annual mean aerosol ERF because the total ERF is commonly used to  
810 quantify the multi-model diversity in historically forced changes to the climate (Myhre et al., 2013; pp661). However, regional  
811 variations in aerosol forcing can be important drivers of climate variability (Chalmers et al., 2012; Booth et al., 2012; Bollasina  
812 et al., 2013; Shindell et al., 2013; Kirtman et al., 2013) and can contribute to global mean forcing uncertainty in complex  
813 ways (Regayre et al., 2015). Therefore we now use satellite observations of the North Pacific (region R1; latitude 32N-54N;  
814 longitude 125W-144E) ToA RSR from July to further constrain annual, global mean aerosol ERF uncertainty.

815

816 The regionally averaged CERES observed ToA RSR is  $162.8 \text{ W m}^{-2}$  (CERES, 2017) with an estimated uncertainty of  $\pm 2\%$   
817 (Hartmann et al., 2013, 2.3.1, pp181). The original sample of one million model variants is reduced to around 10% by applying  
818 the North Pacific July mean RSR constraint and to just 0.5% of the original sample by applying both the global mean and  
819 North Pacific constraints together (Table A4). In combination with the global mean observation, the North Pacific RSR con-  
820 straint has little additional effect on the credible forcing ranges ( $-2.30$  to  $-0.56 \text{ W m}^{-2}$  compared to  $-2.37$  to  $-0.59 \text{ W m}^{-2}$ ). The  
821 range of plausible aerosol ERF values has been further reduced by only around 2%. This suggests that the regional observation  
822 has provided little additional constraint on the relationships between aerosol ERF and the main sources of uncertainty (Fig. S1).

823

## 824 4 Conclusions

825 We sampled the uncertainty in 18 aerosol and 9 atmospheric parameters within a single global climate model, identified the  
826 important causes of aerosol ERF uncertainty and constrained this uncertainty using ToA radiative flux measurements. The  
827 credible range of aerosol ERF values in our original sample of one million model variants was  $-2.65$  to  $-0.68 \text{ W m}^{-2}$  when we  
828 assume the parameter values have equal likelihood of being at any point in the elicited ranges. The aerosol ERF uncertainty de-  
829 creases when we constrain global mean ToA RSR ( $-2.37$  to  $-0.59 \text{ W m}^{-2}$ ) and when we constrain both North Pacific and global  
830 RSR ( $-2.30$  to  $-0.56 \text{ W m}^{-2}$ ). However, a greater reduction (25%) in the aerosol ERF uncertainty (95% credible range,  $-2.18$  to  
831  $-0.71 \text{ W m}^{-2}$ ) can be achieved by applying probability distributions to the parameters based on expert elicitation. These results  
832 suggest that the strongest aerosol ERF values (about 20% of the unconstrained range) can be considered implausible based on



833 expert opinion and observational evidence.

834

835 Our results reveal that aerosol parameters take a dominant role over atmospheric parameters as the leading cause of aerosol  
836 ERF uncertainty over the industrial period and in recent decades. Atmospheric parameters cause the majority (over 80%) of the  
837 uncertainty in present-day ToA reflected short-wave radiation but only around 30% of the aerosol ERF variance. A handful of  
838 the aerosol and atmospheric parameters that we have examined dominate the uncertainty in global mean aerosol ERF. A cloud  
839 radiation parameter, natural aerosol emissions and model process parameters that affect cloud droplet formation and removal  
840 are the key sources of global mean aerosol ERF uncertainty over the industrial period. The most important causes of 1978-2008  
841 aerosol ERF uncertainty are model process parameters controlling the deposition rates of aerosols and aerosol precursor gases.  
842 Our analysis shows that uncertainties in aerosol parameters are of secondary importance for determining present-day ToA  
843 radiative flux, but they are a much more important source (over half) of the uncertainty in the change in atmospheric radiative  
844 balance (the aerosol ERF) on multi-century and multi-decadal timescales.

845

846 Uncertainty in the  $ERF_{ARI}$  component of forcing ( $-0.19$  to  $0.13 \text{ W m}^{-2}$ ) is largely caused by parameters related to car-  
847 bonaceous aerosols. However, these parameters contribute little to uncertainty in the total aerosol ERF, which is dominated by  
848 uncertainty in the  $ERF_{ACI}$  component of forcing ( $-2.20$  to  $0.61 \text{ W m}^{-2}$ ) in our analyses. In our simulations light-absorbing  
849 aerosols heat the local atmosphere above clouds, suppress convection and affect cloud cover. However, we do not represent  
850 all of the processes that determine the magnitude of carbonaceous aerosol forcing. For example, we neglect the deposition  
851 of absorbing-aerosols onto high-albedo land surfaces. Therefore, despite the large uncertainties in our carbonaceous aerosol  
852 parameters, our global mean  $ERF_{ARI}$  uncertainty range does not span the range of values found by Bond et al., 2013.

853

854 At the regional level, uncertainty in aerosol ERF is predominantly caused by the same parameters that cause global mean  
855 aerosol ERF uncertainty. Some parameters such as the cloud radiation parameter `Rad_Mcica_Sigma` and the natural aerosol  
856 emission parameter `DMS` are important for global mean aerosol ERF uncertainty because they cause at least a small amount  
857 (5%) of the uncertainty in nearly all regions. Other important causes of global mean aerosol ERF uncertainty (`Sea_Spray`,  
858 `Sig_W` and `Anth_SO2`) are amongst the largest causes of the aerosol ERF uncertainty in some regions (marine, polluted and  
859 polluted-marine regions respectively) but cause very little of the uncertainty elsewhere. We show that because carbonaceous  
860 aerosols only cause aerosol ERF uncertainty in high-emission months and in regions close to emission sources, most of the  
861 carbonaceous aerosol parameters (with the exception of `Carb_BB_Diam`) are not important for global, annual mean aerosol  
862 ERF uncertainty.

863

864 A well-constrained multi-decadal historical aerosol ERF would provide more policy-relevant information on near-term  
865 temperature change than industrial-period ERF which remains challenging to constrain (Hawkins et al., 2017). Constraining  
866 recent-decadal aerosol ERF uncertainty may prove to be an easier task than constraining uncertainty in industrial-period  
867 forcing because the multi-decadal uncertainty is caused by model process parameters that could be observed directly. Global



868 mean aerosol ERF in recent decades depends more linearly on changing anthropogenic emissions than industrial-period aerosol  
869 ERF. Therefore, the causes of aerosol ERF uncertainty in recent decades (1978-2008) are model deposition rates (model pro-  
870 cess parameters) and anthropogenic emissions, whilst the 1850-2008 aerosol ERF is most sensitive to natural aerosol emissions.  
871 The magnitude of global mean aerosol forcing on the decadal timescale depends on the combination of uncertain positive and  
872 negative regional forcings (Regayre et al. 2015; Fig. 5). Hence, projects designed to improve our understanding of the state  
873 and behaviour of aerosol-cloud-radiation interactions on regional scales and within specific cloud regimes will aid efforts to  
874 constrain global mean forcing. In summary, reducing the uncertainty in aerosol ERF will require a much deeper understanding  
875 of how the uncertainties in state variables, model parameters and the relationships between them combine at the regional and  
876 global levels in complex global climate models. We develop our understanding of the potential to constrain regional aerosol  
877 ERF uncertainty using multiple observable quantities in Johnson et al. (2018).

878

879 Climate models are routinely tuned to match present-day ToA radiative fluxes (in conjunction with multiple other obser-  
880 vational metrics) so as to ensure accurate characterisation of the state of the atmosphere (Kay et al., 2012; Mauritsen et al.,  
881 2012; Flato et al., 2013; Hourdin et al., 2017). Our sensitivity analysis shows that the ToA radiative flux and the 1850-2008  
882 aerosol ERF share common sources of uncertainty. Therefore, observational constraint of ToA flux representing just 0.5% of  
883 the model's prior range has reduced the 95th percent credible interval of our simulated global mean aerosol ERF by around  
884 10%. These results counter the belief that observations of ToA reflected short-wave radiation should not constrain the aerosol  
885 ERF (because RSR values are an order of magnitude larger than the aerosol ERF). However, comprehensively sampling model  
886 uncertainty provides a densely populated multi-dimensional parameter space which connects the observed value (RSR) to the  
887 model variable of interest (the aerosol ERF). The RSR observation constrains the parameter space and in doing so constrains  
888 the aerosol ERF uncertainty. However, we caution that the constraint will only be robust if all relevant parameters affecting  
889 RSR have been explored.

890

891 Our results show that the plausible ranges of individual parameters as well as the relationships between them are constrained  
892 by present-day observations, thereby substantially reducing the model parameter space that can be considered observationally  
893 plausible. We use RSR observations with a small observational uncertainty to demonstrate their potential use as a constraint  
894 on aerosol ERF uncertainty. However, despite a very large reduction in plausible parameter space, the effectiveness of the  
895 observational constraint is modest because it is hampered by compensating effects between multiple uncertain parameters. The  
896 challenge now is to find optimum combinations of constraints that overcome this problem using a more robust framework that  
897 accounts for all quantifiable sources of uncertainty (Sexton et al., 2012; Williamson et al., 2013). For aerosol ERF this means  
898 simultaneously constraining aerosols, clouds, and radiation *state* variables as well as the relationships between them so as to  
899 constrain uncertainty in the *change* of state on multiple timescales.

900

901 By highlighting how different parameters and processes control the change in planetary radiative balance in a single state of  
902 the art model, our results suggest that compensating effects between groups of uncertain parameters and associated processes



903 are one important reason why uncertainty in aerosol ERF has persisted through several generations of climate model develop-  
904 ment. Given the huge range of interacting processes and uncertainties, it is highly unlikely that single observational constraints  
905 (as employed in so-called emergent constraint studies; e.g. Cherian et al. (2014)) will enable a robust reduction in aerosol  
906 ERF uncertainty. Our results, combined with those of other studies that have comprehensively sampled model uncertainties  
907 (Calisto et al., 2014; Lee et al., 2016; Ghan et al., 2016), suggest that reducing aerosol ERF uncertainty further will require the  
908 simultaneous application of a large number of observational constraints (Sanderson, 2010; Sexton et al., 2012; Collins et al.,  
909 2012; Reddington et al., 2017) covering polluted and pristine environments (Carslaw et al., 2013; Hamilton et al., 2014) and  
910 targeting the specific processes and relationships identified here.  
911

## 912 **5 Code availability**

913 Code can be made available upon request from the corresponding author.

## 914 **6 Data availability**

915 Data can be made available upon request from the corresponding author. The authors welcome use of the perturbed parameter  
916 ensemble for advancing climate research.

917 *Author contributions.* L. Regayre tested the model configuration, designed and prepared the ensemble and analysed the results. L. Regayre  
918 and K. Carslaw wrote the article. All authors contributed to the analysis and interpretation of results. K. Pringle, M. Yoshioka, L. Regayre,  
919 K. Carslaw, J. Johnson and N. Bellouin helped prepare the model configuration that served as the template for the ensemble. L. Regayre  
920 and J. Johnson designed the experiments. All simulations were created by L. Regayre. M. Yoshioka advised on computational aspects of the  
921 ensemble creation. The screening of atmospheric parameters was conducted by L. Regayre, D. Sexton and K. Carslaw. L. Regayre and J.  
922 Johnson elicited probability density functions of all aerosol parameters and K. Carslaw, N. Bellouin, K. Pringle, M. Yoshioka and L. Lee  
923 participated (alongside many other experts) in the formal elicitation process.

924 *Competing interests.* The authors declare that they have no conflict of interest.

925 *Acknowledgements.* L. Regayre was funded by a Natural Environment Research Council (NERC) Doctoral Training Grant, and a CASE  
926 studentship with the UK Met Office Hadley Centre. B. Booth was supported by the Joint UK DECC/Defra Met Office Hadley Centre Climate  
927 Programme (GA01101). K. Carslaw is currently a Royal Society Wolfson Merit Award holder. We acknowledge funding from NERC under  
928 grants AEROS, ACID-PRUF, GASSP and A-CURE (NE/G006172/1, NE/I020059/1, NE/J024252/1 and NE/P013406/1). This work and its  
929 contributors (J. Johnson, D. Sexton and K. Carslaw) were supported by the UK-China Research & Innovation Partnership Fund through the  
930 Met Office Climate Science for Service Partnership (CSSP) China as part of the Newton Fund. This work used the ARCHER UK National





931 Supercomputing Service (<http://www.archer.ac.uk>). ARCHER project allocation n02-FREEPPE and the Leadership Project allocation n02-  
932 CCPPE were used to create the ensemble. The authors appreciate the commitment given by participants in the expert elicitation, particularly  
933 C. Johnson, B. Johnson, J. Mollard, S. Turnock, D. Hamilton, A. Schmidt, C. Scott, R. Stevens, E. Butt, C. Reddington, M. Woodhouse, D.  
934 Spracklen and O. Wild.

935 **References**

- 936 Allen, R. J., Norris, J. R., and Kovilakam, M.: Influence of anthropogenic aerosols and the Pacific Decadal Oscillation on tropical belt width,  
937 *Nat. Geosci.*, 7, 270–274, doi:10.1038/NGEO2091, 2014.
- 938 Andreae, M. O., Jones, C. D., and Cox, P. M.: Strong present-day aerosol cooling implies a hot future, *Nat.*, 435, 1187–1190,  
939 doi:doi:10.1038/nature03671, 2005.
- 940 Andrianakis, I., Vernon, I., McCreesh, N., McKinley, T. J., Oakley, J. E., Nsubuga, R. N., Goldstein, M., and White, R. G.: History matching  
941 of a complex epidemiological model of human immunodeficiency virus transmission by using variance emulation, *J. R. Stat. Soc. Ser. C*  
942 *Appl. Stat.*, 66, 717–740, doi:10.1111/rssc.12198, 2017.
- 943 Barker, H. W. and Räisänen, P.: Radiative sensitivities for cloud structural properties that are unresolved by conventional GCMs, *Quart. J.*  
944 *Roy. Meteor. Soc.*, 131, 3103–3122, doi:10.125/qj.04.174, 2005.
- 945 Barrett, T. J., Brattström, S., Sharma, S., Worthy, D. E. J., and Novelli, P.: The role of scavenging in the seasonal transport of black carbon  
946 and sulfate to the Arctic, *Geophys. Res. Lett.*, 38, doi:doi:10.1029/2011GL048221, 2011.
- 947 Bellucci, A., Mariotti, A., and Gualdi, S.: The role of forcings in the Twentieth-Century North Atlantic multidecadal variability: The 1940-  
948 1975 North Atlantic cooling case study, *J. Cli.*, 30, 7317–7337, doi:10.1175/JCLI-D-16-0301.1, 2017.
- 949 Beven, K. and Freer, J.: Equifinality, data assimilation, and uncertainty estimation in mechanistic modelling of complex environmental  
950 systems using the GLUE methodology, *J. Hydrol.*, 249, 11–29, doi:10.1016/S0022-1694(01)00421-8, 2001.
- 951 Bollasina, M. A., Ming, Y., and Ramaswamy, V.: Earlier onset of the Indian monsoon in the late twentieth century: The role of anthropogenic  
952 aerosols, *Geophys. Res. Lett.*, 40, 3715–3720, doi:10.1002/grl.50719, 2013.
- 953 Bond, T. C., Doherty, S. J., Fahey, D. W., Forster, P. M., Berntsen, T., DeAngelo, B. J., Flanner, M. G., Ghan, S., Kärcher, B., Koch, D.,  
954 Kinne, S., Kondo, Y., Quinn, P. K., Sarofim, M. C., Schultz, M. G., Schulz, M., Venkataraman, C., Zhang, H., Zhang, S., Bellouin, N.,  
955 Guttikunda, S. K., Hopke, P. K., Jacobson, M. Z., Kaiser, J. W., Klimont, Z., Lohmann, U., Schwarz, J. P., Shindell, D., Storelvmo, T.,  
956 Warren, S. G., and Zender, C. S.: Bounding the role of black carbon in the climate system: A scientific assessment, *J. Geo. Res. Atmos.*,  
957 118, 5380–5552, doi:10.1002/jgrd.50171, 2013.
- 958 Booth, B. B. B., Dunstone, N. J., Halloran, P. R., Andrews, T., and Bellouin, N.: Aerosols implicated as a prime driver of twentieth-century  
959 North Atlantic climate variability, *Nat.*, 484, 228–232, doi:10.1038/nature10946, 2012.
- 960 Boucher, O., Randall, D., Artaxo, P., Bretherton, C., Feingold, G., Forster, P., Kerminen, V. M., Kondo, Y., Liao, H., Lohmann, U., Rasch,  
961 P., Satheesh, S. K., Sherwood, S., Stevens, B., and Zhang, X. Y.: Clouds and Aerosols, in: *Climate Change 2013: The Physical Science*  
962 *Basis. Contribution of Working Group I to the Fifth Assessment Report of the Intergovernmental Panel on Climate Change*, edited by  
963 Stocker, T. F., Qin, D., Plattner, G. K., Tignor, M., Allen, S. K., Boschung, J., Nauels, A., Xia, Y., Bex, V., and Midgley, P. M., Cambridge  
964 University Press, Cambridge, United Kingdom and New York, USA, 2013.
- 965 Boutle, I. A., Abel, S. J., Hill, P. G., and Morcrette, C. J.: Spatial variability of liquid cloud and rain: observations and microphysical effects,  
966 *Quart. J. Roy. Meteor. Soc.*, 140, 585–594, doi:10.1002/qj.2140, 2014.
- 967 Browse, J., Carslaw, K. S., Arnold, S. R., Pringle, K. J., and Boucher, O.: The scavenging processes controlling the seasonal cycle in Arctic  
968 sulphate and black carbon aerosol, *Atmos. Chem. Phys.*, 12, 6775–6798, doi:10.5194/acp-12-6775-2012, 2012.
- 969 Calisto, M., Folini, D., Wild, M., and Bengtsson, L.: Cloud radiative forcing intercomparison between fully coupled CMIP5 models and  
970 CERES satellite data, *Ann. Geophys.*, 32, 793–807, doi:10.5194/angeo-32-793-2014, 2014.



- 971 Carslaw, K. S., Lee, L. A., Reddington, C. L., Pringle, K. J., Rap, A., Forster, P. M., Mann, G. W., Spracklen, D. V., Woodhouse, M., Regayre,  
972 L. A., and Pierce, J. R.: Large contribution of natural aerosols to uncertainty in indirect forcing, *Nat.*, 503, 67–71, doi:10.1038/nature12674,  
973 2013.
- 974 Carslaw, K. S., Gordon, H., Hamilton, D. S., Johnson, J. S., Regayre, L. A., and Yoshioka, M.: Aerosols in the pre-industrial atmosphere,  
975 *Curr. Clim. Change Rep.*, 3, 1–15, doi:10.101007/s40641-017-0061-2, 2017.
- 976 Carslaw, K. S., Johnson, J. S., Regayre, L. A., and Lee, L. A.: All models are uncertain, but we can do something about it, EOS, TBC, TBC,  
977 doi:TBC, 2018.
- 978 CERES: Clouds and the Earth's Radiant Energy System. [https://ceres.larc.nasa.gov/order\\_data.php](https://ceres.larc.nasa.gov/order_data.php). Accessed: August 2017, [https://ceres.larc.nasa.gov/order\\_data.php](https://ceres.larc.nasa.gov/order_data.php), 2017.
- 979
- 980 Chalmers, N., Highwood, E. J., Hawkins, E., Sutton, R., and Wilcox, L. J.: Aerosol contribution to the rapid warming of near-term climate  
981 under RCP 2.6, *Geophys. Res. Lett.*, 39, L18709, doi:10.1029/2012GL052848, 2012.
- 982 Cherian, R., Quass, J., Salzmann, M., and Wild, M.: Pollution trends over Europe constrain global aerosol forcing as simulated by climate  
983 models, *Geophys. Res. Lett.*, 41, 2176–2181, doi:10.1002/2013GL058715, 2014.
- 984 Collins, M., Booth, B. B. B., Bhaskaran, B., Harris, G. R., Murphy, J. M., Sexton, D. M. H., and Webb, M. J.: Climate model errors, feedbacks  
985 and forcings: a comparison of perturbed physics and multi-model ensembles, *Clim. Dyn.*, 36, 1737–1766, 2010.
- 986 Collins, M., Chandler, R. E., Cox, P. M., Huthnance, J. M., Rougier, J., and Stephenson, D. B.: Quantifying future climate change, *Nat. Clim.*  
987 *Ch.*, 2, 403–409, 2012.
- 988 Collins, M., Knutti, R., Arblaster, J., Dufresne, J. L., Fichefet, D., Friedlingstein, P., Gao, X., Gutowski, W. J., Johns, T., Krinner, G.,  
989 Shongwe, M., Tebaldi, C., Weaver, A. J., and Wehner, M.: Long-term Climate Change: Projections Commitments and Irreversibility, in:  
990 *Climate Change 2013: The Physical Science Basis. Contribution of Working Group I to the Fifth Assessment Report of the Intergovern-*  
991 *mental Panel on Climate Change*, edited by Stocker, T. F., Qin, D., Plattner, G. K., Tignor, M., Allen, S. K., Boschung, J., Nauels, A., Xia,  
992 Y., Bex, V., and Midgley, P. M., Cambridge University Press, Cambridge, United Kingdom and New York, NY, USA, 2013.
- 993 Croft, B., Pierce, J. R., Martin, R. V., Hoose, C., and Lohmann, U.: Uncertainty associated with convective wet removal of entrained aerosols  
994 in a global climate model, *Atmos. Chem. Phys.*, 12, 10 725–10 748, 2012.
- 995 Dunstone, N. J., Smith, D. M., Booth, B. B. B., Hermanson, L., and Eade, R.: Anthropogenic aerosol forcing of Atlantic tropical storms, *Nat.*  
996 *Geosci.*, 6, 534–539, doi:10.1038/ngeo1854, 2013.
- 997 Flato, G., Marotzke, J., Abiodun, B., Braconnot, P., Chou, S. C., Collins, W., Cox, P., Driouech, F., Emori, S., Eyring, V., Forest, C., Glecker,  
998 P., Guilyardi, E., Jacob, C., Kattsov, V., Reason, C., and Rumukainen, M.: Evaluation of Climate Models, in: *Climate Change 2013: The*  
999 *Physical Science Basis. Contribution of Working Group I to the Fifth Assessment Report of the Intergovernmental Panel on Climate*  
1000 *Change*, edited by Stocker, T. F., Qin, D., Plattner, G. K., Tignor, M., Allen, S. K., Boschung, J., Nauels, A., Xia, Y., Bex, V., and Midgley,  
1001 P. M., Cambridge University Press, Cambridge, United Kingdom and New York, USA, 2013.
- 1002 Gantt, B., Johnson, M. S., Crippa, M., Prévôt, A. S. H., and Meskhidze, N.: Implementing marine organic aerosols into the GEOS-Chem  
1003 model, *Geosci. Mod. Dev.*, 8, 619–629, doi:10.5194/gmd-8-619-2015, 2015.
- 1004 Gettleman, A.: Putting the clouds back in aerosol–cloud interactions, *Atmos. Chem. Phys.*, 15, 12 397–12 411, doi:10.5194/acp-15-12397-  
1005 2015, 2015.
- 1006 Gettleman, A., Kay, J. E., and Fasullo, J. T.: Spatial decomposition of climate feedbacks in the Community Earth System Model, *J. Cli.*, 26,  
1007 3544–3561, doi:10.1175/JCLI-D-12-00497.1, 2013.



- 1008 Ghan, S. J.: Technical Note: Estimating aerosol effects on cloud radiative forcing, *Atmos. Chem. Phys.*, 13, 9971–9974, doi:10.5194/acp-13-  
1009 9971-2013, 2013.
- 1010 Ghan, S. J., Wang, M., Zhang, S., Ferrachat, S., Gettleman, A., Griesfeller, J., Kipling, Z., Lohmann, U., Morrison, H., Neubauer, D.,  
1011 Partridge, D. G., Stier, P., Takemura, T., Wang, H., and Zhang, K.: Challenges in constraining anthropogenic aerosol effects on cloud  
1012 radiative forcing using present-day spatiotemporal variability, *Proc. Natl. Acad. Sci.*, 113, 5804–5811, doi:10.1073/pnas.1514036113,  
1013 2016.
- 1014 Gnanadesikan, A., Scott, A. A., Pradal, M. A., and Seviour, W. J. M.: Regional responses to black carbon aerosols: The importance of air-sea  
1015 interaction, *J. Geo. Res. Atmos.*, 122, 12 982–12 999, doi:10.1002/2017JD027589, 2017.
- 1016 Golaz, J. C., Horowitz, L. W., and II, H. L.: Cloud tuning in a coupled climate model: impact on 20th century warming, *Geophys. Res. Lett.*,  
1017 pp. 1–20, 2013.
- 1018 Goldstein, M. and Rougier, J.: Probabilistic formulations for transferring inferences from mathematical models to physical systems, *siam*,  
1019 26, 467–487, doi:10.1137/S106482750342670X, 2004.
- 1020 Gordon, H., Kirkby, J., Baltensperger, U., Bianchi, F., Breitenlechner, M., Curtius, J., Dias, A., Dommen, J., Donahue, N. M., Dunne, E. M.,  
1021 Duplissy, J., Ehrhart, S., Flagan, R. C., Frege, C., Fuchs, C., Hansel, A., Hoyle, C. R., Kulmala, M., Kurten, A., Lehtipalo, K., Makhmutov,  
1022 V., Molteni, U., Rissanen, M. P., Stozkhov, Y., Trostl, J., Tsagkogeorgas, G., Wagner, R., Williamson, C., Wimmer, D., Winkler, P. M.,  
1023 Yan, C., and Carslaw, K. S.: Causes and importance of new particle formation in the present-day and preindustrial atmospheres, *J. Geo.*  
1024 *Res. Atmos.*, 122, 8739–8760, doi:10.1002/2017JD026844, 2017.
- 1025 Granier, C., Bessagnet, B., Bond, T., D’Angiola, A., van der Gon, H. D., Frost, G. J., Heli, A., Kaiser, J. W., Kinne, S., Kilmont, Z., Kloster, S.,  
1026 Lamarque, J. F., Lioussé, C., Masui, T., Meleux, F., Mieville, A., Ohara, T., Raut, J. C., Riahi, K., Schultz, M. G., Smith, S. J., Thompson,  
1027 A., van Aardenne, J., van der Werf, G. R., and van Vuuren, D. P.: Evolution of anthropogenic and biomass burning emissions of air  
1028 pollutants at global and regional scales during the 1980–2010 period, *Climatic Change*, 109, 163–190, doi:10.1007/s10584-011-0154-1,  
1029 2011.
- 1030 Gryspeerdt, E., Quaas, J., Ferrachat, S., Gettelman, A., Ghan, S., Lohmann, U., Morrison, H., Neubauer, D., Partridge, D. G., Stier, P.,  
1031 Takemura, T., Wang, H., Wang, M., and Zhang, K.: Constraining the instantaneous aerosol influence on cloud albedo, *Proc. Natl. Acad.*  
1032 *Sci.*, 114, 4899–4904, doi:10.1073/pnas.1617765114, 2017.
- 1033 Guo, L., Highwood, E. J., Shaffrey, L. C., and Turner, A. G.: The effect of regional changes in anthropogenic aerosols on rainfall of the East  
1034 Asian Sumer Monsoon, *Atmos. Chem. Phys.*, 13, 1521–1534, doi:10.5194/acp-13-1521-2013, 2013.
- 1035 HadCRUT4: Met Office Hadley Centre observations dataset, HadCRUT4. <https://www.metoffice.gov.uk/hadobs/hadcrut4>. Accessed: Oc-  
1036 tober 2017, 2017.
- 1037 HadGEM3: Met Office climate prediction model: HadGEM3 family. [http://www.metoffice.gov.uk/research/modelling-systems/unified-](http://www.metoffice.gov.uk/research/modelling-systems/unified-model/climate-models/hadgem3)  
1038 [model/climate-models/hadgem3](http://www.metoffice.gov.uk/research/modelling-systems/unified-model/climate-models/hadgem3). Accessed: March 2017, 2017.
- 1039 Haerter, J. O., Roeckner, E., Tomassini, L., and von Storch, J. S.: Parametric uncertainty effects on aerosol radiative forcing, *Geophys. Res.*  
1040 *Lett.*, 36, L15707, doi:10.1029/2009GL039050, 2009.
- 1041 Hamilton, D. S., Lee, L. A., Pringle, K. J., Reddington, C. L. S., Spracklen, D. V., and Carslaw, K. S.: Occurrence of pristine aerosol on a  
1042 polluted planet, *Proc. Natl. Acad. Sci.*, 111, 18 466–18 471, doi:10.1073/pnas.1415440111, 2014.
- 1043 Hartmann, D. L., A. M. G. Klein T., Rusticucci, M., Alexander, L. V., Brönnimann, S., Charabi, Y., Dentener, F. J., Dlugokencky, E. J.,  
1044 Easterling, D. R., Kaplan, A., Soden, B. J., Thorne, P. W., Wild, M., and Zhai, P. M.: Observations: Atmosphere and Surface, in: *Climate*  
1045 *Change 2013: The Physical Science Basis. Contribution of Working Group I to the Fifth Assessment Report of the Intergovernmental*



- 1046 Panel on Climate Change, edited by Stocker, T. F., Qin, D., Plattner, G. K., Tignor, M., Allen, S. K., Boschung, J., Nauels, A., Xia, Y.,  
1047 Bex, V., and Midgley, P. M., Cambridge University Press, Cambridge, United Kingdom and New York, NY, USA, 2013.
- 1048 Hawkins, E., Ortega, P., Suckling, E., Schurer, A., Hergl, G., Jones, P., Joshi, M., Osborne, T., Masson-Delmotte, V., Mignot, J., Thorne,  
1049 P., and Jan van Oldenborgh, G.: Estimating changes in global temperature since the preindustrial period, *Bull. Amer. Meteor. Soc.*, pp.  
1050 1841–1856, doi:10.1175/BAMS-D-16-0007.1, 2017.
- 1051 Hetzel, J.: Package ‘Trapezoid’, <https://cran.r-project.org/web/packages/trapezoid/trapezoid.pdf>, 2012.
- 1052 Hourdin, F., Mauritsen, T., Gettleman, A., Golaz, J., Balaji, V., Duan, Q., Folini, D., Klocke, D. J. D., Qian, Y., Rauser, F., Rio, C.,  
1053 Tomassini, L., Watanabe, M., and Williamson, D.: The art and science of climate model tuning, *B. Am. Meteorol. Soc.*, 98, 589–602,  
1054 doi:10.1175/BAMS-D-15-00135.1, 2017.
- 1055 Johnson, J. S., Cui, Z., Lee, L. A., Gosling, J. P., Blyth, A. M., and Carslaw, K. S.: Evaluating uncertainty in convective cloud microphysics  
1056 using statistical emulation, *J. Adv. Model. Earth Syst.*, 7, 162–187, doi:10.1002/2014NS000383, 2015.
- 1057 Johnson, J. S., Regayre, L. A., Yoshioka, M., Pringle, K. J., Lee, L. A., Sexton, D., Rostron, J., Booth, B. B. B., and Carslaw, K. S.: The  
1058 importance of comprehensive parameter sampling and multiple observations for robust constraint of aerosol radiative forcing, *Atmos.*  
1059 *Chem. Phys.*, 18, TBC, doi:TBC, 2018.
- 1060 Karydis, V. A., Tsimpidi, A. P., Bracer, S., Pozzer, A., Nenes, A., and Lelieveld, J.: Global impact of mineral dust on cloud droplet number  
1061 concentration, *Atmos. Chem. Phys.*, 17, 5601–5621, doi:10.5194/acp-17-5601-2017, 2017.
- 1062 Kasoar, M., Voulgarakis, A., Lamarque, J.-F., Shindell, D. T., Bellouin, N., Collins, W. J., Faluvego, G., and Tsigaridis, K.: Regional and  
1063 global temperature response to anthropogenic SO<sub>2</sub> emissions from China in three climate models, *Atmos. Chem. Phys.*, 16, 9785–9804,  
1064 doi:10.5194/acp-16-9785-2016, 2016.
- 1065 Kay, J. E., Hillman, B. R., Klein, S. A., Zhang, Y., Medeiros, B., Pincus, R., Gettleman, A., Eaton, B., Boyle, J., Marchand, R., and Ackerman,  
1066 T. P.: Exposing Global Cloud Biases in the Community Atmosphere Model (CAM) Using Satellite Observations and Their Corresponding  
1067 Instrument Simulators, *J. Cli.*, 25, 5190–5207, doi:10.1175/JCLI-D-11-00469.1, 2012.
- 1068 Khain, A. P., Ovtchinnikov, M., Pinsky, M., Potrovsky, A., and Krugliak, H.: Notes on state-of-the-art numerical modeling of cloud micro-  
1069 physics, *Atmos. Res.*, 55, 159–224, doi:10.1016/S0169-8095(00)00064-8, 2000.
- 1070 Kim, D., Chin, M., Yu, H. B., Diehl, T., Tan, Q., Kahn, R. A., Tsigaridis, K., Bauer, S. E., Takemura, T., Pozzoli, L., Bellouin, N., Schulz, M.,  
1071 Peyridieu, S., Chedin, A., and Koffi, B.: Sources, sinks and transatlantic transport of North African dust aerosol: A multimodel analysis  
1072 and comparison with remote sensing data, *J. Geo. Res. Atmos.*, 119, 6259–6277, doi:10.1002/2013JD021099, 2014.
- 1073 Kipling, Z., Stier, P., Johnson, C. E., Mann, G. W., Bellouin, N., Bauer, S. E., Bergman, T., Chin, M., Diehl, T., Ghan, S. J., Iversen, T.,  
1074 Kirkevåg, A., Kokkola, H., Liu, X. H., Luo, G., von Noije, T., Pringle, K. J., von Salzen, K., Schulz, M., Seland, O., Skeie, R. B.,  
1075 Takemura, T., Tsigaridis, K., and Zhang, K.: What controls the vertical distribution of aerosol? Relationships between process sensitivity  
1076 in HadGEM3-UKCA and inter-model variation from AeroCom Phase II, *Atmos. Chem. Phys.*, 16, 2221–2241, doi:10.5194/acp-16-2221-  
1077 2016, 2016.
- 1078 Kirtman, B., Power, S. B., Adedoyin, J. A., Boer, G. J., Bojariu, R., Camilloni, I., Doblas-Reyes, F. J., Fiore, A. M., Kimoto, M., Meehl, G. A.,  
1079 Prather, M., Sarr, A., Schär, C., Sutton, R., van Oldenborgh, G. J., Vecchi, G., and Wang, H. J.: Near-term Climate Change: Projections  
1080 and Predictability, in: *Climate Change 2013: The Physical Science Basis. Contribution of Working Group I to the Fifth Assessment Report*  
1081 *of the Intergovernmental Panel on Climate Change*, edited by Stocker, T. F., Qin, D., Plattner, G. K., Tignor, M., Allen, S. K., Boschung,  
1082 J., Nauels, A., Xia, Y., Bex, V., and Midgley, P. M., Cambridge University Press, Cambridge, United Kingdom and New York, NY, USA,  
1083 2013.



- 1084 Knutti, R., Krähenmann, S., Frame, D. J., and Allen, M. R.: Comment on “Heat capacity, time constant, and sensitivity of earth’s climate  
1085 system” by SE Schwartz”, *J. Geo. Res. Atmos.*, 113, 1984–2012, doi:10.1029/2007JD009473, 2008.
- 1086 Knutti, R., Masson, D., and Gettleman, A.: Climate model genealogy: Generation CMIP5 and how we got there, *Geophys. Res. Lett.*, 40,  
1087 1194–1199, doi:10.1002/grl.50256, 2013.
- 1088 Koffi, B., Schulz, M., Breon, F. M., Dentener, F., Steensen, B. M., Griesfeller, J., Winker, D., Balkanski, Y., Bauer, S. E., Bellouin, N.,  
1089 Berntsen, T., Bian, H. S., Chin, M., Diehl, T., Easter, R., Ghan, S., Hauglustaine, D. A., Iversen, T., Kirkevåg, A., Liu, X. H., Lohmann,  
1090 U., Myhre, G., Rasch, P., Seland, O., Skeie, R. B., Steenrod, S. D., Stier, P., Tackett, J., Takemura, T., Tsigaridis, K., Vuolo, M. R.,  
1091 Yoon, J., and Zhang, K.: Evaluation of the aerosol vertical distribution in global aerosol models through comparison against CALIOP  
1092 measurements: AeroCom phase II results, *J. Geo. Res. Atmos.*, 121, 7254–7283, doi:10.1002/2015JD024639, 2016.
- 1093 Kooperman, G. J., Pritchard, M. S., Ghan, S. J., Wang, M., Somerville, R. C. J., and Russell, L. M.: Constraining the influence of natural  
1094 variability to improve estimates of global aerosol indirect effects in a nudged version of the Community Atmosphere Model 5, *J. Geo.*  
1095 *Res.*, 117, 1–16, doi:10.1029/2012JD018588, 2012.
- 1096 Korhonen, H., Carslaw, K. S., Spracklen, D. V., Mann, G. W., and Woodhouse, M. T.: Influence of oceanic dimethyl sulfide emissions on  
1097 cloud condensation nuclei concentrations and seasonality over the remote Southern Hemisphere oceans: A global model study, *J. Geo.*  
1098 *Res.*, 113, 16, 2008.
- 1099 Kretzschmar, J., Salzmann, M., Mülmenstädt, J., Boucher, O., and Quass, J.: Comment on “Rethinking the Lower Bound on Aerosol Radia-  
1100 tive Forcing, *J. Cli.*, 30, 6579–6584, doi:10.1175/JCLI-D-16-0668.1, 2017.
- 1101 Lacagnina, C., Hasekamp, O. P., Huisheng, B., Curci, G., Myhre, G., van Noije, T., Schulz, M., Skeie, R. B., Takemura, T., and Zhang, K.:  
1102 Aerosol single-scattering albedo over the global oceans: Comparing PARASOL retrievals with AERONET, OMI, and AeroCom models  
1103 estimates, *J. Geo. Res. Atmos.*, 120, 9814–9836, doi:10.1002/2015JD023501, 2015.
- 1104 Lamarque, J. F., Bond, T. C., Eyring, V., Granier, C., Heli, A., Kilmont, Z., Lee, D., Liou, S. C., Mieville, A., Owen, B., Schultz, M. G.,  
1105 Shindell, D., Smith, S. J., Stehfest, E., Van Aardenne, J., Cooper, O. R., Kainuma, M., Mahowald, N., McConnell, J. R., Naik, V., Riahi,  
1106 K., and van Vuuren, D. P.: Historical (1850–2000) gridded anthropogenic and biomass burning emissions of reactive gases and aerosols:  
1107 methodology and application, *Atmos. Chem. Phys.*, 10, 7017–7039, doi:10.5194/acp-10-7017-2010, 2010.
- 1108 Lebo, Z. J. and Feingold, G.: On the relationship between responses in cloud water and precipitation to changes in aerosol, *Atmos. Chem.*  
1109 *Phys.*, 14, 11 817–11 831, doi:10.5194/acp-14-11817-2014, 2014.
- 1110 Lee, L. A., Carslaw, K. S., Pringle, K. J., Mann, G. W., and Spracklen, D. V.: Emulation of a complex global aerosol model to quantify  
1111 sensitivity to uncertain parameters, *Atmos. Chem. Phys.*, 11, 12 253–12 273, doi:10.5194/acp-11-12253-2011, 2011.
- 1112 Lee, L. A., Carslaw, K. S., Pringle, K. J., and Mann, G. W.: Mapping the uncertainty in global CCN using emulation, *Atmos. Chem. Phys.*,  
1113 12, 9739–9751, doi:10.5194/acp-12-9739-2012, 2012.
- 1114 Lee, L. A., Pringle, K. J., Reddington, C. L., Mann, G. W., Stier, P., Spracklen, D. V., Pierce, J., and Carslaw, K. S.: The magnitude and  
1115 causes of uncertainty in global model simulations of cloud condensation nuclei, *Atmos. Chem. Phys.*, 13, 8879–8914, doi:10.5194/acp-  
1116 13-8879-2013, 2013.
- 1117 Lee, L. A., Reddington, C. L., and Carslaw, K. S.: On the relationship between aerosol model uncertainty and radiative forcing uncertainty,  
1118 *Proc. Natl. Acad. Sci.*, 113, 5820–5827, doi:10.1073/pnas.1507050113, 2016.
- 1119 Liu, X. H. and Wang, J. A.: How important is organic aerosol hygroscopicity to aerosol indirect effect?, *Environ. Res. Lett.*, 5, 044 010,  
1120 doi:10.1088/1748-9326/5/4/044010, 2010.





- 1121 Liu, Y. and Gupta, H. V.: Uncertainties in hydrologic modeling: Toward an integrated data assimilation framework, *Water Resour. Res.*, 43,  
1122 1–17, doi:10.1029/2006WR005756, 2007.
- 1123 Loeb, N. G., Wielicki, B. A., Doelling, D. R., Smith, G. L., Keyes, D. F., Kato, S., Manalo-Smith, N., and Wong, T.: Toward Optimal Closure  
1124 of the Earth's Top-of-Atmosphere Radiation Budget, *J. Climate.*, 22, 748–766, doi:10.1175/2008JCLI2637.1, 2009.
- 1125 Loeb, N. G., Kato, S., Su, W., Wong, T., Rose, F. G., Doelling, D. R., Norris, J. R., and Huang, X.: Advances in Understanding Top-of-  
1126 Atmosphere Radiation Variability from Satellite Observations, *Surv. Geophys.*, 33, 359–385, doi:10.1007/s10712-012-9175-1, 2012.
- 1127 Lohmann, U.: Why does knowledge of past aerosol forcing matter for future climate change?, *J. Geo. Res. Atmos.*, 122, 5021–5023,  
1128 doi:10.1002/2017JD026962, 2017.
- 1129 Lohmann, U. and Ferrachat, S.: Impact of parametric uncertainties on the present-day climate and on the anthropogenic aerosol effect, *Atmos.*  
1130 *Chem. Phys.*, 10, 11 373–11 383, 2010.
- 1131 Malavelle, F. F., Haywood, J. M., Ones, A. J., Gettleman, A., Larisse, L. C., Bauduin, S., Allan, R. P., Karset, I. H. H., Kristjansson, J. E.,  
1132 Oreopoulos, L., Ho, N. C., Lee, D., Bellouin, N., Boucher, O., Grosvenor, D. P., Carslaw, K. S., Dhomse, S., Mann, G. W., Schmidt, A.,  
1133 and M. E. Hartley, H. C., Dalvi, M., Hill, A. A., Johnson, B. T., Johnson, C. E., Knight, J. R., Jeff, R., O'Connor, F. M., Partridge, D. G.,  
1134 Stier, P., Myhre, G., Platnick, S., Stephens, G. L., Takahashi, H., and Thordarson, T.: Strong constraints on aerosol-cloud interactions from  
1135 volcanic eruptions, *Nat.*, 543, 485–491, doi:10.1038/nature22974, 2017.
- 1136 Manktelow, P. T., Carslaw, K. S., Mann, G. W., and Spracklen, D. V.: The impact of dust on sulfate aerosol, CN and CCN during an East  
1137 Asian dust storm, *Atmos. Chem. Phys.*, 10, doi:10.5194/acp-10-365-2010, 2010.
- 1138 Mann, G. W., Carslaw, K. S., Spracklen, D. V., Ridley, D. A., Manktelow, P. T., Chipperfield, M. P., Pickering, S. J., and Johnson, C. E.:  
1139 Description and evaluation of GLOMAP-mode aerosol microphysics model for the UKCA composition-climate model, *Geosci. Mod.*  
1140 *Dev.*, 3, 519–551, doi:10.5194/gmd-3-519-2010, 2010.
- 1141 Mann, G. W., Carslaw, K. S., Reddington, C. L., Pringle, K. J., Schulz, M., Asmi, A., Spracklen, D. V., Ridley, D. A., Woodhouse, M. T., Lee,  
1142 L. A., Zhang, K., Ghan, S. J., Easter, R. C., Liu, X., Stier, P., Lee, Y. H., Adams, P. J., Tost, H., and S. E. Bauer, J. L., Tsigaridis, K., van  
1143 Noije, T. P. C., Strunk, A., Vignati, E., Bellouin, N., Dalvi, M., Johnson, C. E., Bergman, T., Kokkola, H., von Salzen, K., Yu, F., Luo, G.,  
1144 Petzold, A., Heizenberg, J., Clarke, A., Ogren, A., Gras, J., Baltensperger, U., Kaminski, U., Jennings, S. G., O'Dowd, C. D., Harrison,  
1145 R. M., Beddows, D. C. S., Kulmala, M., Viisanen, Y., Ulevicius, V., Mihalopoulos, N., Zdimal, V., Fiebig, M., Hansson, H., Swietlicki,  
1146 E., and Henzing, J. S.: Intercomparison and evaluation of global aerosol microphysical properties among AeroCom models of a range of  
1147 complexity, *Atmos. Chem. Phys.*, 14, 4679–4713, doi:10.5194/acp-14-4679-2014, 2014.
- 1148 Mauritsen, T., Stevens, B., Roeckner, E., Crueger, T., Esch, M., Giorgetta, M., Haak, H., Jungclaus, J., Klocke, D., Matei, D., Mikolajewicz,  
1149 U., Notz, D., Pincus, R., Schmidt, H., and Tomassini, L.: Tuning the climate of a global model, *J. Adv. Model. Earth Syst.*, 4, M00A01,  
1150 doi:10.1029/2012MS000154, 2012.
- 1151 Metzger, A., Verheggen, B., Dommen, J., Duplissy, J., Prevot, A. S. H., Weingartner, E., Riipinen, I., Kulmala, M., Spracklen, D. V., Carslaw,  
1152 K. S., and Baltensperger, U.: Evidence for the role of organics in aerosol particle formation under atmospheric conditions, *Proc. Natl. Acad.*  
1153 *Sci.*, 107, 6646–6651, doi:10.1073/pnas.0911330107, 2010.
- 1154 Michibata, T. and Takemura, T.: Evaluation of autoconversion schemes in a single model framework with satellite observations, *J. Geo. Res.*  
1155 *Atmos.*, 120, 1–21, doi:10.1002/2015JD023818-T, 2015.
- 1156 Morgan, M. G., Adams, P. J., and Keith, D. W.: Elicitation of expert judgements about aerosol forcing, *Clim. Change.*, 75, 195–214,  
1157 doi:10.1007/s10584-005-9025-y, 2006.



- 1158 Myhre, G., Shindell, D., Bréon, F. M., Collins, W., Fuglestedt, J., Huang, J., Koch, D., Lamarque, J. F., Lee, D., Mendoza, B., Nakajima,  
1159 T., Robock, A., Stephens, G., Takemura, T., and Zhang, H.: Anthropogenic and Natural Radiative Forcing, in: *Climate Change 2013:*  
1160 *The Physical Science Basis. Contribution of Working Group I to the Fifth Assessment Report of the Intergovernmental Panel on Climate*  
1161 *Change*, edited by Stocker, T. F., Qin, D., Plattner, G. K., Tignor, M., Allen, S. K., Boschung, J., Nauels, A., Xia, Y., Bex, V., and Midgley,  
1162 P. M., Cambridge University Press, Cambridge, United Kingdom and New York, NY, USA, 2013.
- 1163 Nam, C., Bony, S., Dufresne, J. L., and Chepfer, H.: The ‘too few, too bright’ tropical low-cloud problem in CMIP5 models, *Geophys. Res.*  
1164 *Letts.*, 39, L21 801, doi:10.1029/2012GL053421, 2012.
- 1165 Neubauer, D., Lohmann, U., Hoose, C., and Frontoso, M. G.: Impact of the representation of marine stratocumulus clouds on the anthro-  
1166 pogenic aerosol effect, *Atmos. Chem. Phys.*, 14, 11 997–12 022, doi:10.5194/acp-14-11997-2014, 2014.
- 1167 Oakley, J. E. and O’Hagan, A.: Probabilistic sensitivity analysis of complex models: a Bayesian approach, *JRSSB*, 66, 751–769, 2004.
- 1168 Pan, X., Chin, M., Gautam, R., Bian, H., Kim, D., Colarco, P. R., Diehl, T. L., Takemura, T., Pozzoli, L., Tsigaridis, K., Bauer, S., and  
1169 Bellouin, N.: A multi-model evaluation of aerosols over South Asia: common problems and possible causes, *Atmos. Chem. Phys.*, 15,  
1170 5903–5928, doi:10.5194/acp-15-5903-2015, 2015.
- 1171 Pennell, C. and Reichler, T.: On the effective number of climate models, *J. Cli.*, 24, 2358–2367, 2010.
- 1172 Petters, M. D. and Kreidenweis, S. M.: A single parameter representation of hygroscopic growth and cloud condensation nucleus activity,  
1173 *Atmos. Chem. Phys.*, 7, 1961–1971, doi:10.5194/acp-7-1961-2007, 2007.
- 1174 Pianosi, F., Beven, K., Freer, J., Hall, J. W., Rougier, J., Stephenson, D. B., and Wagener, T.: Sensitivity analysis of environmental models:  
1175 A systematic review of practical workflow, *Environ. Mod. Soft.*, 79, 214–232, doi:10.1016/j.envsoft.2016.02.008, 2016.
- 1176 Pringle, K. J., Carslaw, K. S., Fan, T., Mann, G. W., Hill, A., Stier, P., Zhang, K., and Tost, H.: A multi-model assessment of the impact of  
1177 sea spray geoengineering on cloud droplet number, *Atmos. Chem. Phys.*, 12, 11 647–11 663, 2012.
- 1178 Qian, Y., Yan, H., Zhangshuan, H., Gardar, J., Klein, S., Lucas, D., Neale, R., Rasch, P., Swiller, L., Tannahill, J., Wang, H., Wang, M., and  
1179 Zhao, C.: Parametric sensitivity analysis of precipitation at global and local scales in the Community Atmosphere Model CAM5, *J. Adv.*  
1180 *Model. Earth Syst.*, 7, 382–411, doi:10.1002/2014MS000354, 2015.
- 1181 Räisänen, P., Barker, H. W., Khairoutdinov, M. F., Li, J., and Randall, D. A.: Stochastic generation of subgrid-scale cloudy columns for  
1182 large-scale models, *Quart. J. Roy. Meteor. Soc.*, 130, 2047–2067, doi:10.125/qj.03.99, 2004.
- 1183 Randles, C. A., Kinne, S., Myhre, G., Schulz, M., Stier, P., Fisher, J., Doppler, L., Highwood, E., Ryder, C., Harris, B., Huttunen, J., Ma,  
1184 Y., Pinker, R. T., Mayer, B., Neubauer, D., Hitzenberger, R., Oreopoulos, L., Lee, D., Pitari, G., Di Genova, G., Quaas, J., Rose, F. G.,  
1185 Kato, S., Rumbold, S. T., Vardavas, I., Hatzianastassiou, N., Matsoukas, C., Yu, H., Zhang, F., Zhang, H., and Lu, P.: Intercomparison  
1186 of shortwave radiative transfer schemes in global aerosol modeling: results from the AeroCom Radiative Transfer Experiment, *Atmos.*  
1187 *Chem. Phys.*, 13, 2347–2379, doi:10.5194/acp-13-2347-2013, 2013.
- 1188 Reddington, C. L., Carslaw, K., Spracklen, D., Frontoso, M., Collins, L., Merikanto, J., Minikin, A., Hamburger, T., Coe, H., Kulmala,  
1189 M., Aalto, P., Flentje, H., Plass-Dulmer, C., Birmili, W., Wiedensohler, A., Wehner, B., Tuch, T., Sonntag, A., O’Dowd, C., Jennings,  
1190 S., Dupuy, R., Baltensperger, U., Weingartner, E., Hansson, H., Turned, P., Laj, P., Skellegri, K., Boulton, J., Putaud, J., Gruening, C.,  
1191 Swietlicki, E., Roldin, P., Henzing, J., Moerman, M., Mihalopoulos, N., Kouvarakis, G., Zdimal, V., Zikova, N., Marinoni, A., Bosasoni,  
1192 P., and Duchi, R.: Primary versus secondary contributions to particle number concentrations in the European boundary layer, *Atmos.*  
1193 *Chem. Phys.*, 11, 12 007–12 036, 2011.
- 1194 Reddington, C. L., Carslaw, K. S., Stier, P., Schutgens, N., Coe, H., Liu, D., Allan, J., Browse, J., Pringle, K., Lee, L., Yoshioka, M., Johnson,  
1195 J., Regayre, L., Spracklen, D., Mann, G., Clarke, A., Hermann, M., Henning, S., Wex, H., Kristensen, T., Leitch, W., Poeschl, U., Rose,



- 1196 D., Andreae, M., Schmale, J., Kondo, Y., Oshima, N., Schwarz, J., Nenes, A., Andreson, B., Roberts, G., Snider, J., Leck, C., Quinn, P.,  
1197 Chi, X., Ding, A., Jimenez, J., and Zhang, Q.: The Global Aerosol Synthesis and Science Project (GASSP), *B. Am. Meteorol. Soc.*, In  
1198 Press, doi:10.1175/BAMS-D-15-00317.1, 2017.
- 1199 Regayre, L. A., Pringle, K. J., Booth, B. B. B., Lee, L. A., Mann, G. W., Browse, J., Woodhouse, M. T., Rap, A., Reddington, C. L. S., and  
1200 Carslaw, K. S.: Uncertainty in the magnitude of aerosol-cloud radiative forcing over recent decades, *Geophys. Res. Lett.*, 41, 9040–9049,  
1201 doi:10.1002/2014GL062029, 2014.
- 1202 Regayre, L. A., Pringle, K. J., Lee, L. A., Booth, B. B. B., Rap, A., Browse, J., Mann, G. W., Woodhouse, M. T., Reddington, C. L. S., and  
1203 Carslaw, K. S.: The climatic importance of uncertainties in regional aerosol-cloud radiative forcings over recent decades, *J. Climate.*, 28,  
1204 6589–6607, doi:10.1175/JCLI-D-15-0127.1, 2015.
- 1205 Reutter, P., Su, H., Trentmann, J., Simmel, M., Rose, D., Gunthe, S. S., Wernli, H., Andreae, M. O., and Pöschl, U.: Aerosol- and updraft-  
1206 limited regimes of cloud droplet formation: influence of particle number, size and hygroscopicity on the activation of cloud condensation  
1207 nuclei CCN, *Atmos. Chem. Phys.*, 9, 7067–7080, doi:10.5194/acp-9-7067-2009, 2009.
- 1208 Rodrigues, L. F. S., Vernon, I., and Bower, R.: Constraints on galaxy formation models from the galaxy stellar mass function and its evolution,  
1209 *Mon. Not. R. Astron. Soc.*, 466, 2418–2435, doi:10.1093/mnras/stw3269, 2017.
- 1210 Rougier, J.: Ensemble averaging and mean squared error, *J. Cli.*, 29, 8865–8870, doi:10.1175/JCLI-D-16-0012.1, 2016.
- 1211 Saltelli, A., Tarantola, S., and Chan, K. P. S.: A quantitative model-independent method for global sensitivity analysis of model output,  
1212 *Technometrics*, 41, 39–56, doi:10.2307/1270993, 1999.
- 1213 Saltelli, A., Chan, K., and Scott, E. M.: *Sensitivity Analysis*, Wiley, Oxford, U.K., 2000.
- 1214 Samset, B. H., Myhre, G., Herber, A., Kondo, Y., Li, S. M., Moteki, N., Koike, M., Oshima, N., Schwarz, J. P., Balkanski, Y., Bauer, S. E.,  
1215 Bellouin, N., Bernsten, T. K., Bian, H., Chin, M., Diehl, T., Easter, R. C., Ghan, S. J., Iversen, T., Kirkevåg, A., Lamarque, J. F., Lin, G.,  
1216 Liu, X., Penner, J. E., Schulz, M., Seland, O., Skeie, R. B., Stier, P., Takemura, T., and Zhang, K. T. K.: Modelled black carbon radiative  
1217 forcing and atmospheric lifetime in AeroCom Phase II constrained by aircraft observations, *Atmos. Chem. Phys.*, 14, 12465–12477,  
1218 doi:10.5194/acp-14-12465-2014, 2014.
- 1219 Sanderson, B. M.: A multimodel study of parametric uncertainty in predictions of climate response to rising greenhouse gas concentrations.,  
1220 *J. Climate.*, 24, 1362–1377, doi:10.1175/2010JCLI3498.1, 2010.
- 1221 Schmidt, A., Ostro, B., Carslaw, K. S., Wilson, M., Thordarson, T., Mann, G. W., and Simmons, A. J.: Excess mortality in Europe following  
1222 a future Laki-style Icelandic eruption, *Proc. Natl. Acad. Sci.*, 108, 15710–15715, 2011.
- 1223 Schulz, M., Textor, C., Kinne, S., Balkanski, Y., Bauer, S., Bernsten, T., Berglen, T., Boucher, O., Dentener, F., Guibert, S., Isaksen, I. S. A.,  
1224 Iversen, T., Koch, D., Kirkevåg, A., Liu, X., Montanaro, V., Myhre, G., Penner, J. E., Pitari, G., Reddy, S., Seland, O., Stier, P., and  
1225 Takemura, T.: Radiative forcing by aerosols as derived from the AeroCom present-day and pre-industrial simulations, *Atmos. Chem.*  
1226 *Phys.*, 6, 5225–5246, 2006.
- 1227 Schutgens, N., Tsyro, S., Gryspeerdt, E., Goto, D., Weigum, N., Schulz, M., and Stier, P.: On the spatio-temporal representativeness of  
1228 observations, *Atmos. Chem. Phys.*, 17, 9761–9780, doi:10.5194/acp-17-9761-2017, 2017.
- 1229 Seinfeld, J. H., Bretherton, C., Carslaw, K. S., Coe, H., DeMott, P. J., Dunlea, E. J., Feingold, G., Ghan, S., Guenther, A. B., Kahn, R.,  
1230 Kraucunas, I., Kreidenweis, S. M., Molina, M. J., Nenes, A., Penner, J. E., Prather, K. A., Ramanathan, V., Ramaswamy, V., Rasch, P. J.,  
1231 Ravishankara, A. R., Rosenfeld, D., Stephens, G., and Wood, R.: Improving our fundamental understanding of the role of aerosol-cloud  
1232 interactions in the climate system, *Proc. Natl. Acad. Sci.*, 113, 5781–5790, doi:10.1073/pnas.1514043113, 2016.



- 1233 Sexton, D. M. H., Murphy, J. M., Collins, M., and Webb, M. J.: Multivariate probabilistic projections using imperfect climate models Part I:  
1234 outline of methodology, *Clim. Dyn.*, 38, 2513–2542, 2012.
- 1235 Sexton, D. M. H., Karmalkar, A., Murphy, J., and Booth, B. B. B.: The elicitation of distributions of parameters in HadGEM3 versions GA4  
1236 and GA7 for use in perturbed parameter ensembles, Hadley Centre technical note 101, Met Office, U.K., 2018.
- 1237 Shindell, D. T., Lamarque, J. F., Schulz, M., Flaner, M., Jiao, C., Chin, M., Young, P., Lee, Y., Rotstayn, L., Mahowald, N., Milly, G.,  
1238 Faluvegi, G., Balkanski, Y., Collins, W. J., Conley, A. J., Dalsoren, S., Easter, R., Ghan, S., Horowitz, L., Liu, X., Myhre, G., Nagashima,  
1239 T., Naik, V., Rumbold, S. T., Skeie, R., Sudo, K., Szopa, S., Takemura, T., Voulgarakis, A., Yoon, J. H., and Lo, F.: Radiative forcing in  
1240 the ACCMIP historical and future climate simulations, *Atmos. Chem. Phys.*, 13, 2939–2974, doi:10.5194/acp-13-2939-2013, 2013.
- 1241 Shiogama, H., Watanabe, M., Yoshimori, M., Yokohata, T., Ogura, T., Annan, J. D., Hargreaves, J. C., Abe, M., Kamae, Y., O’ishi, R., Nobui,  
1242 R., Emori, S., Nozawa, T., Abe-Ouchi, A., and Kimoto, M.: Perturbed physics ensemble using the MIROC5 coupled atmosphere-ocean  
1243 GCM without flux corrections: experimental design and results, *Clim. Dyn.*, 39, 3041–3056, doi:10.1007/s00382-012-1441-x, 2012.
- 1244 Shrivastava, M., Zhao, C., Easter, R. C., Qian, Y., Zelenyuk, A., Fast, J. D., Liu, Y., Zhang, Q., and Guenther, A.: Sensitivity analysis of  
1245 simulated SOA loadings using a variance-based statistical approach, *J. Adv. Model. Earth Syst.*, 8, 499–519, doi:10.1002/2015MS000554,  
1246 2016.
- 1247 Smith, S. J., van Aardenne, J., Klimont, Z., Andres, R. J., Volke, A., and Arias, S. D.: Anthropogenic sulfur dioxide emissions: 1850 to 2005,  
1248 *Atmos. Chem. Phys.*, 11, 1101–1116, doi:10.5194/acp-11-1101-2011, 2011.
- 1249 Snedecor, G. W. and Cochran, W. G.: *Statistical methods*, Iowa State University Press, 8th edn., 1989.
- 1250 Spracklen, D. V., Pringle, K. J., Carslaw, K. S., Chipperfield, M. P., and Mann, G. W.: A global off-line model of size-resolved aerosol  
1251 microphysics: I. Model development and prediction of aerosol properties, *Atmos. Chem. Phys.*, 5, 2227–2252, doi:10.5194/acp-5-2227-  
1252 2005, 2005.
- 1253 Spracklen, D. V., Carslaw, K. S., Merikanto, J., Mann, G. W., Reddington, C. L., Pickering, S., Ogren, J. A., Andrews, E., Baltensperger,  
1254 U., Weingartner, E., Boy, M., Kulmala, M., Laakso, L., Lihavainen, H., Kivekas, N., Komppula, M., Mihalopoulos, N., Kouvarakis, G.,  
1255 Jennings, S., O’Dowd, C., Birmili, W., Wiedensohler, A., Weller, R., Gras, J., Laj, P., Sellegri, K., Bonn, B., Krejci, R., Laaksonen, A.,  
1256 Hamed, A., Minikin, A., Harrison, R. M., Talbot, R., and Sun, J.: Explaining global surface aerosol number concentrations in terms of  
1257 primary emissions and particle formation, *Atmos. Chem. Phys.*, 10, 4775–4793, 2010.
- 1258 Spracklen, D. V., Carslaw, K. S., Pöschl, U., Rap, A., and Forster, P.: Global cloud condensation nuclei influenced by carbonaceous combus-  
1259 tion aerosol, *Atmos. Chem. Phys.*, 11, 9067–9087, doi:10.5194/acp-11-9067-2011, 2011a.
- 1260 Spracklen, D. V., Jimenez, J. L., Carslaw, K. S., Worsnop, D. R., Evans, M. J., Mann, G. W., Zhang, Q., Canagaratna, M. R., Allan, J., Coe,  
1261 H., McFiggans, G., Rap, A., and Forster, P.: Aerosol mass spectrometer constraint on the global secondary organic aerosol budget, *Atmos.*  
1262 *Chem. Phys.*, 11, 12 109–12 136, doi:10.5194/acp-11-12109-2011, 2011b.
- 1263 Stevens, B.: Rethinking the Lower Bound on Aerosol Radiative Forcing, *J. Cli.*, 28, 4794–4819, doi:10.1175/JCLI-D-14-00656.1, 2015.
- 1264 Stevens, B. and Feingold, G.: Untangling aerosol effects on clouds and precipitation in a buffered system, *Nat.*, 461, 607–613, 2009.
- 1265 Stier, P., Schutgens, N. A. J., Bian, H., Boucher, O., Chin, M., Ghan, S., Huneus, N., Kinne, S., Lin, G., Myhre, G., Penner, J. E., Randles, C.,  
1266 Samset, B., Schulz, M., Yu, H., and Zhou, C.: Host model uncertainties in aerosol radiative forcing estimates: results from the AeroCom  
1267 prescribed intercomparison study, *Atmos. Chem. Phys.*, 13, 3245–3270, doi:10.5194/acp-13-3245-2013, 2013.
- 1268 Storelvmo, T., Lohmann, U., and Bennartz, R.: What governs the spread in shortwave forcings in the transient IPCC AR4 models?, *Geophys.*  
1269 *Res. Lett.*, 36, doi:10.1029/2008GL036069, 2009.



- 1270 Sullivan, S. C., Lee, D., Oreopoulos, L., and Nenes, A.: Role of updraft velocity in temporal variability of global cloud hydrometeor number,  
1271 Proc. Natl. Acad. Sci., 113, 5791–5796, doi:10.1073/pnas.1514039113, 2016.
- 1272 Taylor, K. E., Stouffer, R. J., and Meehl, G. A.: An Overview of CMIP5 and the Experiment Design, Bull. Amer. Meteor. Soc., 93, 485–498,  
1273 doi:10.1175/BAMS-D-11-00094.1, 2012.
- 1274 Telford, P. J., Braesicke, P., Morgenstern, O., and Pyle, J. A.: Technical Note: Description and assessment of a nudged version of the new  
1275 dynamics Unified Model, Atmos. Chem. Phys., 8, 1701–1712, doi:tbc, 2008.
- 1276 Tett, S. F. B., Rowlands, D. J., Mineter, M. J., and Cartis, C.: Can Top-Of-Atmosphere Radiation Measurements Constrain Climate Predic-  
1277 tions? Part II: Climate Sensitivity, J. Climate., 26, 9367–9383, doi:10.1175/JCLI-D-12-00596.1, 2013.
- 1278 Textor, C., Schulz, M., Guibert, S., Kinne, S., Balkanski, Y., Bauer, S., Berntsen, T., Berglen, T., Boucher, O., Chin, M., Dentener, F., Diehl,  
1279 T., Easter, R., Feichter, H., Fillmore, D., Ghan, S., Ginoux, P., Gong, S., Grini, A., Hendricks, J., Horowitz, L., Huang, P., Isaksen, I.,  
1280 Iversen, I., Kloster, S., Koch, D., Kirkevåg, A., Kristjansson, J. E., Krol, M., Lauer, A., Lamarque, J. F., Liu, X., Montanaro, V., Myhre,  
1281 G., Penner, J., Pitari, G., Reddy, S., Seland, O., Stier, P., Takemura, T., and Tie, X.: Analysis and quantification of the diversities of aerosol  
1282 life cycles within AeroCom, Atmos. Chem. Phys., 6, 1777–1813, doi:10.5194/acp-6-1777-2006, 2006.
- 1283 Textor, C., Schulz, M., Guibert, S., Kinne, S., Balkanski, Y., Bauer, S., Berntsen, T., Berglen, T., Boucher, O., Chin, M., Dentener, F., Diehl,  
1284 T., Feichter, J., Fillmore, D., Ginoux, P., Gong, S., Grini, A., Hendricks, J., Horowitz, L., Huang, P., Isaksen, I. S. A., Iversen, T., Kloster,  
1285 S., Koch, D., Kirkevåg, A., Kristjansson, J. E., Kro, M., Lauer, A., Lamarque, J. F., Liu, X., Montanaro, V., Myhre, G., Penner, J. E.,  
1286 Pitari, G., Reddy, M. S., Seland, O., Stier, P., Takemura, T., and Tie, X.: The effect of harmonized emissions on aerosol properties in  
1287 global models - an AeroCom experiment, Atmos. Chem. Phys., 7, 4489–4501, doi:10.5194/acp-7-4489-2007, 2007.
- 1288 Torrence, C. and Compo, G.: A practical guide to wavelet analysis, Bull. Am. Meteorol. Soc., 79, 61–78, 1998.
- 1289 Tost, H., Lawrence, M. G., Brühl, C., and Jöckel, P.: Uncertainties in atmospheric chemistry modelling due to convection parameterisations  
1290 and subsequent scavenging, Atmos. Chem. Phys., 10, 1931–1951, 2010.
- 1291 Tsigaridis, K., Daskalakis, N., Kanakidou, M., Adams, P. J., Artaxo, P., Bahadur, R., Balkanski, Y., Bauer, S. E., Bellouin, N., Benedetti, A.,  
1292 Bergman, T., Berntsen, T. K., Beukes, J. P., Bian, H., Carslaw, K. S., Chin, M., Curci, G., Diehl, T., Easter, R. C., Ghan, S. J., Gong, S. L.,  
1293 Hodzic, A., Hoyle, C. R., Iversen, T., Jathar, S., Jimenez, J. L., Kaiser, J. W., Kirkevåg, A., Koch, D., Kokkola, H., Lee, Y. H., Lin, G., Liu,  
1294 X., Luo, G., Ma, X., Mann, G. W., Mihalopoulos, N., J.-J.Morcrette, J.-F.Müller, Myhre, G., Myriokefalitakis, S., Ng, N. L., O'Donnell,  
1295 D., Penner, J. E., Pozzoli, L., Pringle, K. J., Russell, L. M., Schulz, M., Sciare, J., Seland, O., Shindell, D. T., Sillman, S., Skeie, R. B.,  
1296 Spracklen, D., Stavroukou, T., Steenrod, S. D., Takemura, T., Titta, P., Tilmes, S., Tost, H., van Noije, T., van Zyl, P. G., von Salzen, K., Yu,  
1297 F., Wang, Z., Wang, Z., Zaveri, R. A., Zhang, H., Zhang, K., Zhang, Q., and Zhang, X.: The AeroCom evaluation and intercomparison of  
1298 organic aerosol in global models, Atmos. Chem. Phys., 14, 10 845–10 895, doi:10.5194/acp-14-10845-2014, 2014.
- 1299 van der Werf, G. R., Randerson, J. T., Giglio, L., Collatz, G. J., Mu, M., Kasibhatla, P. S., Norton, D. C., DeFries, R. S., Jin, Y., and van  
1300 Leeuwen, T. T.: Global fire emissions and the contribution of deforestation, savanna, forest, agricultural, and peat fires (1997-2009),  
1301 Atmos. Chem. Phys., 10, 11 707–11 735, doi:10.5194/acp-10-11707-2010, 2010.
- 1302 Vehkamäki, H., Kulmala, M., Napari, I., Lehtinen, K. E. J., Timmreck, C., Noppel, M., and Laaksonen, A.: An improved parameterization  
1303 for sulfuric acid-water nucleation rates for tropospheric and stratospheric conditions, J. Geo. Res., 107, doi:10.1029/2002JD002184, 2002.
- 1304 Vergara-Temprado, J., Murray, B. J., Wilson, T. W., O'Sullivan, D., Browse, J., Pringle, K. J., Ardon-Dryer, K., Bertram, A. K., Burrows,  
1305 S. M., Ceburnis, D., DeMott, P. J., Mason, R. H., O'Dowd, C., Rinaldi, M., and Carslaw, K. S.: Contribution of feldspar and marine organic  
1306 aerosols to global ice nucleating particle concentrations, Atmos. Chem. Phys., 17, 3637–3658, doi:10.5194/acp-17-3637-2017, 2017.



- 1307 Villarini, G. and Vecchi, G. A.: Projected increases in North Atlantic tropical cyclone intensity from CMIP5 models, *J. Cli.*, 26, 3231–3240,  
1308 doi:10.1175/JCLI-D-12-00441.1, 2013.
- 1309 Welch, B. L.: The generalization of ‘Student’s’ problem when several different population variances are involved, *Biometrika*, 34, 28–35,  
1310 doi:10.1093/biomet/34.1-2.28, 1947.
- 1311 West, R. E. L., Stier, P., Jones, A., Johnson, C. E., Mann, G. W., Bellouin, N., Partridge, D. G., and Kipling, Z.: The importance of vertical  
1312 velocity variability for estimates of the indirect aerosol effects, *Atmos. Chem. Phys.*, 14, 6369–6393, doi:10.5194/acp-14-6369-2014,  
1313 2014.
- 1314 Wilcox, L. J., Highwood, E. J., Booth, B. B. B., and Carslaw, K. S.: Quantifying sources of inter-model diversity in the cloud albedo effect,  
1315 *Geophys. Res. Lett.*, 42, 1568–1575, doi:10.1002/2015GL063301, 2015.
- 1316 Williamson, D., Goldstein, M., Allison, L., Blaker, A., Challenor, P., Jackson, L., and Yamazaki, K.: History matching for exploring  
1317 and reducing climate model parameter space using observations and a large perturbed physics ensemble, *Clim. Dyn.*, 41, 1703–1729,  
1318 doi:10.1007/s00382-013-1896-4, 2013.
- 1319 Yoshioka, M., Regayre, L. A., Pringle, K. J., Johnson, J. S., Mann, G. W., Partridge, D., Stier, P., Kipling, Z., Bellouin, N., Sexton, D. M. H.,  
1320 Lister, G. M. S., Browse, J., Booth, B. B. B., Johnson, C. E., Johnson, B., Mollard, J. D. P., and Carslaw, K. S.: Ensembles of global  
1321 climate model variants for the quantification and constraint of uncertainty in aerosols and their radiative forcing, *J. Adv. Model. Earth*  
1322 *Syst.*, TBC, TBC, In prep.
- 1323 Zhang, S., Wang, M., Ghan, S., Ding, A., Wang, H., Zhang, K., Neubauer, D., Lohmann, U., Ferrachat, S., Takeamura, T., Gettleman, A.,  
1324 Morrison, H., Lee, Y. H., Shindell, D. T., Partridge, D. G., Stier, P., Kipling, Z., and Fu, C.: On the characteristics of aerosol indirect effect  
1325 based on dynamic regimes in climate models, *Atmos. Chem. Phys. Discuss.*, 15, 23 683–23 729, doi:10.5194/acpd-15-23683-2015, 2015.
- 1326 Zhou, C., Liu, X., Qian, Y., Yoon, J., Hou, Z., Lin, G., McFarlane, S., Wang, H., Yang, B., L. Ma, P., Yan, H., and Bao, J.: A sensitivity study  
1327 of radiative fluxes at the top of the atmosphere to cloud-microphysics and aerosol parameters in the community atmosphere model CAM5,  
1328 *Atmos. Chem. Phys.*, 13, 10 969–10 987, doi:10.5194/acp-13-10969-2013, 2013.





**Table A1.** Descriptions of the perturbed parameters. Parameters are grouped according to their source within the model as either ‘Atm’ for atmospheric or ‘Aer’ for aerosol parameters.

Name	Source	Description	PDF
Rad_Mcica_Sigma	Atm	Fractional standard deviation of sub-grid condensate seen by radiation	Trapezoid (0.1,0.4,1.5,2.2,2,2)
C_R_Correl	Atm	Cloud and rain sub-grid horizontal spatial correlation	Trapezoid (0.0, 0.6, 0.9, 1.0, 1.8, 1, 1, 1.5)
Niter_Bs	Atm	Number of microphysics iteration sub-steps	Uniform (5, 20)
Ent_Fac_Dp	Atm	Entrainment amplitude scale factor	Trapezoid (0, 0.5, 2, 4, 2, 2)
Amdet_Fac	Atm	Mixing detrainment rate scale factor	Trapezoid (0, 0.5, 10.0, 15.0, 2, 2)
Dbsdtbs_Turb_0	Atm	Cloud erosion rate ( $s^{-1}$ )	Trapezoid (0, 1e-04, 5e-04, 1e-03, 2, 2)
Mparwtr	Atm	Maximum value of function controlling convective parcel maximum condensate	Trapezoid (1e-3, 1e-3, 1.5e-3, 2e-3, 2, 2)
Dec_Thres_Cld	Atm	Threshold for cloudy boundary layer decoupling	Trapezoid (0.01, 0.011, 0.1, 0.8, 2, 4, 4)
Fac_Qsat	Atm	Rate of change in convective parcel maximum condensate	Uniform (0.25, 1)
Ageing	Aer	Ageing of hydrophobic aerosols (no. of monolayers of organic material)	Trapezoid (0.3, 1, 5, 10, 2, 2)
Cloud_pH	Aer	pH of cloud droplets	Trapezoid (4.6, 5.3, 6.3, 7, 4, 2)
Carb_BB_Ems	Aer	Carbonaceous biomass burning emission scale factor	Trapezoid (0.25,0.8,2.2,4,2,2)
Carb_BB_Diam	Aer	Carbonaceous biomass burning emission diameter (nm)	Trapezoid (90, 160, 240, 300, 2, 2)
Sea_Spray	Aer	Sea spray aerosol emission scale factor	Trapezoid (0.125, 0.6, 3, 8, 4, 3)
Anth_SO2	Aer	Anthropogenic SO <sub>2</sub> emission scale factor	Trapezoid (0.6, 0.81, 1.09, 1.5, 2, 2)
Volc_SO2	Aer	Volcanic SO <sub>2</sub> emission scale factor	Trapezoid (0.71, 0.99, 1.7, 2.38, 4, 1.1)
BVOC_SOA	Aer	Biogenic secondary aerosol formation from volatile organic compounds scale factor	Trapezoid (0.81, 1.08, 3.5, 5.4, 3, 3)
DMS	Aer	Dimethylsulphide surface ocean SO <sub>2</sub> concentration scale factor	Trapezoid (0.5, 1.26, 1.82, 2, 2, 3)
Dry_Dep_Acc	Aer	Accumulation mode dry deposition velocity scale factor	Trapezoid (0.1, 0.32, 3.16, 10, 2, 2)
Dry_Dep_SO2	Aer	SO <sub>2</sub> dry deposition velocity scale factor	Trapezoid (0.2, 0.56, 1.78, 5, 2, 2)
Kappa_OC	Aer	Köhler coefficient of organic carbon	Trapezoid (0.1, 0.14, 0.25, 0.6, 4, 4)
Sig_W	Aer	Updraft vertical velocity standard deviation	Trapezoid (0.1, 0.36, 0.44, 0.7, 2, 2)
Dust	Aer	Dust emission scale factor	Trapezoid (0.5, 0.7, 1.4, 2, 2, 2)
Rain_Frac	Aer	Fraction of cloud covered area in large-scale clouds where scavenging occurs	Trapezoid (0.3, 0.31, 0.55, 0.7, 2, 3)
Cloud_Ice_Thresh	Aer	Threshold of cloud ice fraction above which nucleation scavenging is suppressed	Trapezoid (0.1, 0.105, 0.35, 0.5, 2, 3)
BC_RI	Aer	Imaginary part of the black carbon refractive index	Trapezoid (0.2, 0.352, 0.616, 0.8, 4, 2)
OC_RI	Aer	Imaginary part of the organic carbon refractive index	Trapezoid (0, 0, 0.05, 0.1, 2, 6)



**Table A2.** Summary statistics for the pdfs of 1850-2008 aerosol ERF,  $ERF_{ARI}$  and  $ERF_{ACI}$  presented in Fig. 1. Perturbations to atmospheric and/or aerosol parameters cause the uncertainty in model output in each case. All values are in  $Wm^{-2}$ . For all samples the null hypotheses of equivalent means or standard deviations are rejected at the 99% confidence level using Welch's t (Welch, 1947) and Bartlett (Snedecor and Cochran, 1989) tests respectively.

Sample	Perturbations	Mean	Standard deviation	95% Credible interval	Credible range
ERF	Atmosphere and aerosol	-1.46	0.38	(-2.18, -0.71)	1.46
	Atmosphere only	-1.51	0.25	(-1.98, -1.04)	0.94
	Aerosol only	-1.47	0.29	(-2.01, -0.90)	1.11
$ERF_{ARI}$	Atmosphere and aerosol	-0.03	0.08	(-0.19, 0.13)	0.31
	Atmosphere only	0.00	0.04	(-0.08, 0.08)	0.16
	Aerosol only	-0.02	0.07	(-0.16, 0.11)	0.27
$ERF_{ACI}$	Atmosphere and aerosol	-1.42	0.41	(-2.20, -0.61)	1.59
	Atmosphere only	-1.51	0.29	(-2.04, -0.96)	1.08
	Aerosol only	-1.43	0.30	(-1.99, -0.85)	1.14



**Table A3.** Latitude and longitude boundaries for regions R1-R11. Some regional averages are filtered to include only marine or non-marine data.

Region	Description	Filter	Latitudes	Longitudes
R1	North Pacific	Marine	32.5 to 54	144 to -125
R2	East Pacific Stratocumulus Deck	Marine	16 to 41	-146 to -104
R3	Canada	All	45 to 73	-115 to -61
R4	South-east Pacific Stratocumulus deck	Marine	-26 to 1	-98 to -70
R5	North Atlantic	Marine	27 to 59	-53 to -12
R6	South-east North Atlantic	Marine	8.5 to 26	-44 to -17
R7	Arctic	Marine	61 to 89	-33 to 57
R8	Europe	All	37.5 to 71.5	-12 to 41
R9	South-east Atlantic Stratocumulus deck	Marine	-18 to 3	-16 to 13
R10	North Indian Ocean	Marine	5.5 to 23	63 to 94
R11	China	Land	21 to 40	98 to 123



**Table A4.** Present-day ToA RSR constraints and the resulting 95% credible intervals of 1850 RSR and 1850-2008 aerosol ERF ( $\text{W m}^{-2}$ ) for the unconstrained and constrained samples.

Constraint	Sample size	2008 RSR	1850 RSR	1850-2008 ERF	1850-2008 ERF credible range
Unconstrained	1000000	(88.9, 120.1)	(87.5, 118.0)	(-2.65, -0.68)	1.97
CERES ( $98.3 \pm 0.25 \text{ W m}^{-2}$ )	20127	(98.05, 98.55)	(94.2, 99.3)	(-2.37, -0.59)	1.78
CERES North Pacific ( $162.8 \pm 3.3 \text{ W m}^{-2}$ )	108493	(89.6, 106.8)	(88.0, 105.1)	(-2.25, -0.53)	1.72
Combined constraint	4699	(98.1, 98.5)	(95.7, 97.8)	(-2.30, -0.56)	1.74